Forschungszentrum Karlsruhe

in der Helmholtz-Gemeinschaft

Wissenschaftliche Berichte

FZKA 6822
SAM-COLOSS-P055

Analytical Support for the B_4C Control Rod Test QUENCH-07

Ch. Homann, W. Hering, J. Birchley[1], J. A. Fernández Benítez[2],
M. Ortega Bernardo[2]

Institut für Reaktorsicherheit

[1] Paul Scherrer Institut, Switzerland
[2] Universidad Politécnica de Madrid, Spain

Forschungszentrum Karlsruhe GmbH, Karlsruhe
2003

Impressum der Print-Ausgabe:

Als Manuskript gedruckt

Forschungszentrum Karlsruhe GmbH
Postfach 3640, 76021 Karlsruhe

Mitglied der Hermann von Helmholtz-Gemeinschaft
Deutscher Forschungszentren (HGF)

ISSN 0947-8620

Abstract

Degradation of B_4C absorber rods during a beyond design accident in a nuclear power reactor may be a safety concern. Among others, the integral test QUENCH-07 is performed in the FZK QUENCH facility and supported by analytical work within the Euratom Fifth Framework Programme on Nuclear Fission Safety to get a more profound database. Since the test differed substantially from previous QUENCH tests, much more work had to be done for pretest calculations than usual to guarantee the safety of the facility and to derive the test protocol. Several institutions shared in this work with different computer code systems, as used for nuclear reactor safety analyses. Due to this effort, problems could be identified and solved, leading to several modifications of the originally planned test conduct, until a feasible test protocol could be derived and recommended. All calculations showed the same trends. Especially the high temperatures and hence the small safety margin for the facility were a concern. In this report, contributions of various authors, engaged in this work, are presented.

The test QUENCH-07 and the related computational support by the engaged institutions were co-financed by the European Community under the Euratom Fifth Framework Programme on Nuclear Fission Safety 1998 – 2002 (COLOSS Project, contract No. FIKS-CT-1999-00002).

Zusammenfassung

Analytische Unterstützung für das B_4C Kontrollstab-Experiment QUENCH-07

Das Versagen von B_4C Absorberstäben bei einem auslegungsüberschreitenden Unfall in einem Kernkraftwerk kann von Bedeutung für die Einhaltung der Sicherheitsrichtlinien sein. Um eine bessere Datenbasis zu bekommen, wird im Rahmen des 5. Rahmenprogramms der Euratom zur Sicherheit der Kernspaltung unter anderem der Integraltest QUENCH-07 in der QUENCH-Anlage des FZK durchgeführt und durch analytische Arbeiten unterstützt. Da sich der Versuch beträchtlich von früheren QUENCH-Versuchen unterschied, mussten viel umfangreichere Vorausrechnungen als sonst gemacht werden, um die Sicherheit der Anlage zu garantieren und den Versuchsablauf festzulegen. An dieser Arbeit haben sich mehrere Forschungseinrichtungen mit unterschiedlichen Rechenprogrammen beteiligt, die für Sicherheitsanalysen von Kernreaktoren benutzt werden. Auf Grund dieser Bemühungen konnten Probleme erkannt und gelöst werden. Es waren mehrere Änderungen am ursprünglich geplanten Versuchsablauf nötig, bis ein endgültiges Testprotokoll festgelegt werden konnte. Alle Rechnungen zeigten ein ähnliches Verhalten. Vor allem die hohen Temperaturen und der dadurch bedingte geringe Sicherheitsspielraum für die Anlage waren ein Problem. In diesem Bericht werden Beiträge von verschiedenen Autoren dargestellt, die für diese Aufgaben im 5. Rahmenprogramm der Europäischen Kommission mitgearbeitet haben.

Der Versuch QUENCH-07 und die zugehörige Unterstützung durch Rechnungen durch die beteiligten Einrichtungen wurden teilweise im 5. Rahmenprogramm der Euroatom zur Sicherheit der Kernspaltung 1998 – 2002 (Projekt COLOSS, Vertragsnummer FIKS-CT-1999-00002) durch die Europäische Union finanziert.

Table of Contents

List of Figures

List of Tables

1 Introduction

Though in a nuclear power reactor the number of absorber elements is small (about 4 %) in comparison to the number of fuel rods, the effects of the degradation of absorber elements in an accident cannot be neglected because of their relatively low melting temperature. During their degradation droplets of hot material are deposited on the cladding of the surrounding fuel rods, and the resulting compounds influence the physical and chemical behaviour of the fuel rods, e.g. by lowering melting points. Besides the formation of gaseous oxidation products of B_4C, especially of CH_4, is of interest for safety considerations for the following reason. When the steam mass flow in the core is small enough, CH_4 may be formed mainly in colder parts of the primary circuit and in the containment; of course, a certain steam mass flow is needed to oxidise B_4C. When fuel rods also fail and fission products are released, CH_4 may be transformed into volatile organic iodine compounds. These compounds cannot be retained appropriately by filters, and hence are a safety concern when released into the environment.

Because of this importance for reactor safety considerations the impact of B_4C absorber rod degradation during a postulated accident in a nuclear power reactor is dealt in the COLOSS Project, which is part of the Euratom Fifth Framework Programme on Nuclear Fission Safety, launched by the European Community. Among others three integral experiments and related pre- and post-test calculations with large severe accident code systems, currently used for safety analyses in nuclear power reactors, are supported and co-financed by the European Community. For VVER-1000 reactor conditions this item is addressed in the CODEX-B4C experiment, performed in the CODEX facility at AEKI /1/, and for Western type reactors in tests QUENCH-07 /2/ and QUENCH-09 /3/, both performed in the QUENCH facility at FZK. In this report, however, only test QUENCH-07 will be addressed.

In detail, test QUENCH-07 is to fulfil two aims. Firstly it should provide experimental data on degradation of B_4C control rods, its impact on surrounding fuel rods, and the production of gas (in particular H_2 and CH_4) before and during reflood in conditions as representative as possible of commercial 1300 MW Pressurized and Boiling Water Reactors (PWR and BWR). Secondly, it should provide a useful database for the preparation of the future PHEBUS FPT3 in-pile experiment /4/. For the last reason, test QUENCH-07 was intended to be run as similar as possible to the planned PHEBUS test FPT3.

Since the projected test differed in more than one aspect from previous QUENCH tests, it was thought prudent to rely on more than one institution and on more than one code system to prepare the test and to determine the test conduct. The aims of these calculations were twofold. They should give a sufficient confidence that the integrity of the QUENCH facility would be maintained in the test, and they should help to optimize the test conduct, so that as much benefit as possible could be drawn from the experiment.

The following institutions participated in pre- and post-test calculations and performed independent calculations for test QUENCH-07, (in alphabetic order of their tokens) Forschungszentrum Karlsruhe (FZK), Germany, with SCDAP/RELAP5, Institut für Kernenergetik und Energiesysteme (IKE) at Stuttgart University, Germany, with ATHLET-CD, Paul Scherrer Institut (PSI), Villigen, Switzerland, with SCDAP/RELAP5, and Universidad Politécnica de Madrid (UPM), Madrid, Spain, with ICARE2. They helped identifying and solving problems

associated with the planning of this test, and many fruitful discussions in the various COLOSS meetings and elsewhere. Especially, between PSI and FZK a close cooperation was initiated, because in both institutions SCDAP/RELAP5 (S/R5) mod 3.2 /5/ was used. In this context, FZK delivered FZK programme changes /6/ and a current input deck to PSI. In fact, however, the two programme versions were somewhat, but not seriously, different. This was intentional, as will be explained later.

Some of the calculations for test QUENCH-07 were made available for this report by engaged institutions. Except for FZK work, they concern pre-test calculations by PSI (section 4) and UPM (section 5). This report is meant to document the large computational effort, which was necessary to perform test QUENCH-07 at least partly. It is also meant to give a first insight of the quality of this work by comparing results, calculated according to the real experimental conditions, with the measured data and identifying open points and needs for further interpretation of the test. The present report shows the status of this analysis work at the end of the COLOSS project. Pre- and post-test calculations by IKE and post-test analysis by PSI will be documented in separate reports by the engaged institutions.

2 Experimental Basis

2.1 QUENCH Facility

In the following a short description of various aspects of the QUENCH facility is given. More details are documented in /2/ and /7/. The QUENCH facility (Fig. 1) consists of the test section as its main part and a number of external devices. The test section consists of a bundle with 21 rods (Fig. 2). Their arrangement and their cladding are typical for commercial Western type PWRs. In test QUENCH-07 the central rod is a control rod, essentially as used in Western type PWRs with a B_4C absorber rod; the absorber rod design is identical to that for the projected PHEBUS test FPT3. The other 20 rods are fuel rod simulators with annular ZrO_2 pellets, heated electrically over a length of 1.024 m; the tungsten heaters are connected to a combination of molybdenum and copper electrodes at both ends. Electrical power supply is independent for the eight inner and the twelve outer rod simulators. The four Zircaloy corner rods are intended to improve thermal-hydraulic conditions in the bundle; in addition, they are used for instrumentation. One of them may be removed during the test to analyze the axial profile of the oxide layer thickness. The bundle is contained in a Zircaloy shroud and insulated by ZrO_2 fibre material. The whole set-up is enclosed in a steel containment.

A mixture of steam and argon enters the bundle from the bottom; the fluid, i.e. steam, argon, hydrogen and other products formed or released in the bundle, leaves the bundle at its top to enter the off-gas pipe. In the cooling jacket, there is a counter-current water flow in the upper electrode zone and a counter-current argon flow in the heated and the lower electrode zone.

The test section up to and including the outer cooling jacket is equipped with nearly 90 thermocouples at 17 axial locations in the heated and in both electrode zones. Fluid composition is mainly analyzed by two quadrupole mass spectrometers in the off-gas pipe downstream of the bundle.

2.2 Original Test Protocol

From the requirements for the test, explained in section 0, a first proposal for the test conduct, the original test protocol (OTP), was derived as outlined in the following. As usual in QUENCH tests, the experiment begins with a stabilisation phase with a constant maximum bundle temperature of about 800 K. In this phase, checks are performed to verify the correct working of the various systems. Temperatures are already at an elevated level, but low enough to avoid premature oxidation. To be as close to FPT3 as possible, a power transient similar to previous QUENCH experiments is applied afterwards. When a maximum bundle temperature of 1500 K is reached, the nominal steam mass flow of 3 g/s, used up to then, is reduced to such a low value that steam starvation occurs in the bundle. As a first guess, “steam starvation” means a steam mass flow of not more than 10 mg/s at the end of the heated zone. Within the limits for maximum bundle temperature increase, normally applied for QUENCH tests, this event should be reached as soon as possible. The test is continued at a constant maximum bundle temperature of about 2000 K for 15 to 20 minutes (plateau phase) before initiating the cool-down phase. During the steam-starved phase, electrical power is assumed still to increase linearly for a certain time as in the projected FPT3 test. Some more details of the test conduct were to be derived from the results of pre-test calculations.

The value for the temperature plateau is chosen to give large chemical reaction rates, but to be sufficiently below clad melting temperature; the limit of 2000 K is perhaps too high because of the second criterion. If clad melting occurred the results would be more difficult to interpret e.g. because of material relocation. If the temperature limit of 2000 K cannot be met, the maximum bundle temperature must not exceed 2200 K in any case to limit rod damage. The time interval of 15 to 20 minutes is suggested to facilitate the detection of the reaction products, also taking in mind that it is not known in advance whether hot material of the control rod is relocated in colder parts of the bundle and for this reason contributes with only small reaction rates.

Based on temperatures measured in previous QUENCH tests it can easily be assessed that CH_4 is only formed in the off-gas pipe. For interpretation of measured data, it should be kept in mind that the fluid temperature varies substantially as well along the off-gas pipe as well as across the flow cross section. Therefore, the CH_4 concentration is supposed not to be constant in the cross section where the probes for the mass spectrometer are taken. For the maximum fluid temperature at the location of the mass spectrometer, the reading of thermocouple T 601 should be representative. Since the fluid velocity in the off-gas pipe is some 10 cm/s it is hoped that the amount of CH_4 is not too far from equilibrium values for the respective temperatures.

3 FZK Calculations

From the very beginning of the project, QUENCH activities have been supported by calculations with SCDAP/RELAP5 (S/R5) /5/ to define experimental parameters of the QUENCH experiments and to interpret the experimental results after the test. For the calculations presented here, the in-house version of S/R5 mod 3.2 has been used; the new code version, mod 3.3, is still inoperable; severe code errors have been reported to the code developers, but user support by the code developer is not any longer available. Among others, the current in-house version contains an improved model for heat transfer in the transition boiling region /8/, an adaptation of the CORA heater rod model to the conditions of the QUENCH facility, and the material property data for ZrO_2 instead of those for UO_2 to model the pellets /6/.

The various calculations also rely on the experience gained from the calculations done for the previous quench tests. Especially the adjustment of the electrical resistance of the circuit outside the electrical heater rods and the adjustment of the thermal conductivity of the shroud insulation, both based on calculations for test QUENCH-01 /9/, were kept.

3.1 Modelling of the QUENCH Facility

The modelling of the QUENCH facility with S/R5 is the same for all tests that are investigated. In the radial direction, the whole facility including the containment is modelled (Fig. 3), because the radial heat losses out of the bundle depend ultimately on the ambient room temperature. This modelling is mandatory for all work performed before experimental data are available, and it is desirable for all post-test analyses, because the calculated data are more detailed than the experimental ones.

The central rod, the two rings of rods to be heated independently, the four Zircaloy corner rods, the inner and outer cooling jacket, and the containment are modelled as SCDAP components. Two-dimensional heat conduction within the structures and radiation between adjacent structures are taken into account. The temperature at the end of the rods is set to 300 K. As a central rod, an unheated fuel rod is modelled for nearly all calculations, the original code model of B_4C absorber rods being rather poor or even inappropriate. Meanwhile, however, the SCDAP model for the PWR control rod was extended for the correct B_4C material property data. B_4C oxidation is not yet taken into account, because before the development of a respective code model further interpretation of separate effect tests at FZK is necessary. Use of this model is mentioned explicitly in the text. The corner rods are modelled as fuel rods; for most calculations, the radius of the ZrO_2 pellets is set to a very small value to model the real geometry realistically. For the electrical resistance of the circuit outside the electrical heater rods the same value of 4.2 mΩ per rod is used as for test QUENCH-01 /9/. The ZrO_2 fibre insulation is modelled to end at the upper end of the heated zone. With this exception, all structures must be modelled to have the same length because of limitations in the code. Therefore, the upper and lower head cannot be modelled in all details.

The bundle flow and the gas atmospheres outside the outer cooling jacket, i.e. in the containment and the laboratory, are represented by a single channel each. The gas atmospheres outside the outer cooling jacket are assumed stagnant, thus neglecting natural convection in these regions. Because of restrictions in the code, where only a limited number of materials can be specified, these atmospheres are modelled to consist of argon.

The off-gas pipe is taken into account with its whole length of 3 m, including the orifice at the position where the gas sample for the mass spectrometer is taken and the orifice at the outlet of the off-gas pipe to simulate correctly the pressure boundary conditions during reflood phase. The mass flows in the off-gas pipe and the adjacent cooling jacket are modelled to be one-dimensional, the structures are modelled as RELAP heat structures, thus taking into account radial heat transfer within the structures.

For most calculations, the region of the heated part is axially modelled with ten 0.1 m long mesh cells. In the lower and upper electrode zones 0.45 and 0.6 m, respectively, of the test section are considered, each by three mesh cells. For the lowermost node in the lower electrode zone copper as electrode material is assumed and molybdenum elsewhere. In addition to this 16 nodes facility (16f) model a 32 nodes facility (32f) model is now available, where the whole facility is modelled as in the 16f model, but all axial mesh lengths as well in the heated zone as well as the electrode zones are halved. Again, copper is assumed as electrode material in the lowermost zone of the lower electrode zone and molybdenum elsewhere. Moreover, the radial discretization of the fuel simulator rods has been refined. Furthermore, a 32 nodes bundle (32b) model has been created as a fast running approximate solution, with all axial mesh lengths as in the 32f model /7/. However, only one SCDAP component is used to simulate all heated rods, and the corner rods are not modelled. The facility outside the cooling flows is not considered. Instead, the flow area for the argon cooling flow is changed artificially to result in realistic radial heat losses out of the bundle. Instead, the flow area for the argon cooling flow is changed artificially to result in realistic radial heat losses out of the bundle. A 16 nodes bundle (16b) model may easily be created, but is not used actually.

3.2 Pre-Test Calculations

3.2.1 Original Test Protocol

Since the begin of test QUENCH-07 is similar to that of test QUENCH-04, the physical initial and boundary conditions simulated in the pre-test calculations are derived from post-test calculations for test QUENCH-04. In detail, the following scenario is assumed for the pre-test calculations. Initial temperatures for all structures are the same as in test QUENCH-04; the temperature at both ends of the heated rods is 300 K during the whole calculation. The reference pressure at the outlet of the off-gas pipe is 0.2 MPa. A bundle inlet temperature of 620 K is assumed for the whole test with a mass flow in the bundle of 3 g/s each for steam and argon for the first part of the test. The argon- and the water-cooling are counter-current flows with mass flow rates of 6 g/s and 100 g/s, respectively, and an inlet temperature of 300 K. A constant power of 3.8 kW is assumed up to t = 100 s to simulate the end of the stabilisation phase. Then a linear power increase with 6 W/s (total value, as measured in the experiment) is assumed, the rod power for the inner and the outer heated rings being as in QUENCH-04. When a maximum bundle temperature of 1500 K is reached, steam mass flow is reduced to 0.4 g/s, the linear power increase is continued. All pre-test calculations were done with the 16f model, the others not being available at that time.

Fig. 4 shows representative results for these pre-test calculations. In the plots for power, label “input” means total input as measured and “elec” means that part of the electrical power, which is released in the bundle. The difference between these two powers is released outside the computational domain, e.g. in the sliding contacts or the wires leading to the power

supply. “oxid” refers to chemical power release. Before steam flow reduction, temperatures in the two uppermost heated levels (12 and 13) are predicted to be similar, as it has also been seen for other QUENCH tests /9/ and /10/. Afterwards, however, level 13 (elevation 0.95 m) is not calculated to become and to remain the hottest level as in previous tests. Instead maximum temperature shifts to lower axial positions. In a similar manner the axial position of maximum oxide layer thickness changes. Hydrogen production rate indicates that practically the whole steam supply is consumed as it is intended.

The changes due to steam flow reduction can well be seen from axial plots in Fig. 5 for the time of steam flow reduction and Fig. 6 for the time, when a maximum temperature of 1900 K is reached. The axial profiles of temperature and oxide layer thickness become flatter after steam flow reduction and shift somewhat to the bundle centre. The shift of the position of maximum hydrogen release is more pronounced and is exactly at the bundle centre at that time. The changes are even more pronounced when a maximum bundle temperature of 2000 K is reached (Fig. 7). The maximum oxide layer thickness is no longer at the end of the heated zone but in the bundle centre. The figures also demonstrate the change of local electrical power input, due to the well-known positive feedback: for electrically heated rods, the electrical resistance increases with temperature and so does the local electrical power. This in turn increases temperature and hence local power release. This effect is still enhanced by oxidation, which increases temperature further.

During the pre-test calculations it was also examined whether the transient to reach the high temperature plateau can be speeded up, when steam flow is reduced at lower temperatures, say when a maximum bundle temperature of 1400 K is reached. Fig. 4 shows that for the nominal steam mass flow rate of 3 g/s temperature increase from 1400 to 1500 K occurs in about 160 s, so that not more than this time can be saved, and this time interval is rather small in comparison to the overall transient time. Therefore, the original plan to reduce the steam mass flow rate when a temperature of 1500 K is reached is retained for further pre-test calculations to compare results better.

3.2.2 Modified Test Protocol

Fig. 4 shows that electrical power cannot continue to increase during the whole plateau phase as assumed here, if a constant maximum bundle temperature is to be obtained. Further calculations show that the electrical power transient should be continued for some time after steam flow reduction only, to reach elevated temperatures as soon as possible, but then be reduced to a much lower value and be kept constant. Otherwise, too high temperatures occur, and even clad melting must be faced before the end of the envisaged duration of the high temperature test phase. A summary of conditions for the pre-test calculations, as described in this and in the previous section, is given in Table 1. Depending on the ideas, underlying the respective calculations, the original value of 0.4 g/s for the steam mass flow rate is not always retained.

The calculations also show that besides to the power history explained above argon flow must be increased for a sufficient heat removal. For technical reasons the argon mass flow in the bundle should not be larger than 8 g/s, a value of 6 g/s being preferred, because the amount of argon supply is limited. Higher values were chosen for some calculations as a first attempt, and for sensibility studies. In sum, these calculations show that the test conduct must be different from that of the planned PHEBUS FPT3 test to achieve the same physical conditions.

During the plateau phase, the bundle reacts sensitively to changes of physical parameters because of the low convective heat transfer; the two cases shown in Fig. 8 differ only by the argon mass flow rate as a test parameter. For a value of 8 g /s, the bundle temperatures in the upper half of the heated zone have a maximum somewhat above 1600 K, whereas temperatures increase steadily for an argon mass flow of 6 g/s. This leads to clad melting, when the plateau phase is longer, and anyway constant temperatures as desired do not occur.

The figure also shows that just after power reduction chemical power due to oxidation has about the same value as electrical power. In contrast to electrical power, which is released into the whole bundle, chemical power release is mainly constrained to a small region in the upper half of the heated zone, and hence local chemical power input exceeds local electrical power input by far. Since maximum temperature depends strongly on local power input, these results demonstrate the limits to influence the behaviour of the bundle by varying global electrical power input.

Since FZK single-effect tests suggest that a higher steam mass flow of, say, 1 g/s might be acceptable to reach the objectives of the test, some higher steam mass flow rates up to 1 g/s were also tested (Table 1). Of course, the steam mass flow rate at the end of the heated section is higher in these cases because total steam consumption in the bundle is only some hundred mg/s according to actual temperature and oxide layer thickness. Besides the rupture strain was decreased, such reducing rod ballooning, which might have been overestimated in previous calculations. Even for the modified test protocol (MTP) with higher steam flow rates the sensitivity of the response on changes of test parameters remains a concern as can be seen from Fig. 9, where electrical heat input during the plateau phase are 5 and 5.5 kW. In one case, temperatures decrease and clad melting occurs in the other case. The sensitivity of the facility, predicted in these calculations, is considered so large that the integrity of the facility cannot be guaranteed. To give an impression of this sensitivity, results for all calculations listed in Table 1 are given in Fig. 10.

3.2.3 Final Test Protocol

Consequently a new test conduct, the final test protocol (FTP) as indicated in Fig. 11, was proposed during the COLOSS topical meeting on QUENCH-07 /4/. It is closer to previous QUENCH tests and consists of five phases, namely

Phase I	Heat-up phase (from the beginning of the test up to about 1500 K)
Phase II	Expected failure of B_4C control rod, B_4C-SS-Zry melt formation and relocation
Phase III	Oxidation of residual B_4C and relocated products under stationary conditions
Phase IV	Delayed oxidation of B, C – containing compounds at high temperature in subsequent transient
Phase V	Cool-down of partially degraded bundle, exposure of non-oxidized B, C – containing materials?

The main difference to the previous test protocols is the phase after reaching elevated temperatures, which shall now be performed with nominal steam mass flow. In addition, some specifications of the test conduct are fixed in more detail than before. Clad temperature in-

crease is limited to 0.3 – 0.5 K/s during test phase II to guarantee a benign temperature increase and so to minimize the risk of temperature escalations and premature rod damage. Furthermore, details of the cool-down phase are specified.

It was agreed to perform three sets of pre-test calculations. The first one should be performed exactly according to Fig. 11; test phase IV should be achieved by increase of electrical power input at constant steam mass flow rate of 3 g/s. The second one should be done with test phase III to be extended to 15 to 20 minutes. The third one should be performed with constant electrical power and reduced steam flow during test phase IV to such a value that steam starvation is obtained in the bundle at least before cool-down initiation.

For a better organisation of the work, first calculations were done for test phases I to III only, in this way combining the first and second computational set for those test phases. The limitation of temperature increase before reaching the high temperature plateau implies a different power history than assumed for the previous suggestion for test conduct. Firstly, the original power increase of 6 W/s has to be reduced to 4 W/s, when a maximum bundle temperature of 1100 K is reached. Secondly, electrical power has to be increased stepwise when the maximum bundle temperature is above 1700 K to compensate the decrease of chemical power release due to oxidation, which occurs with increasing oxide layer thickness. Maintaining the high temperature plateau over a sufficiently long time, but keeping maximum temperature below clad melting point, proved to be another laborious work, above all because of the high temperature level and hence the small safety margin for the facility. Fig. 12 shows the effort to be done for this purpose. When clad melting temperature is reached in the corner rods, temperature oscillations at values about 2100 K are calculated, not only for the corner rods but also for the heated rods (Fig. 12). They are due to a code weakness, when the pellet radius is much smaller than usual for normal fuel rods (see section 4.2.2). It can be circumvented when some small artificial geometry change is made for the corner rods.

Similar to Fig. 10 for the previous test protocols, this figure also gives an impression of predicted sensitivity of the facility with respect to changes of electrical power input showing that even minor changes decide about clad melting or an acceptable temperature range during test phase III. This sensitivity was confirmed by the experimental results of test QUENCH-09 /3/, when compared to QUENCH-07 /2/. This justifies the large analytical effort to define the test conduct with hindsight.

The calculation labelled “final” shows that a temperature plateau of about 1800 K can be maintained for 20 minutes without difficulties except for a careful tuning of electrical power input. In internal discussions at FZK a maximum oxide layer thickness of 400 µm at the end of test phase III was considered reasonable in the sense that effects expected in the following phases, mainly oxidation, should be sufficiently large. Therefore test phase III is restricted to 15 minutes and ends at 4000 s. Axial profiles of relevant data at that time are given in Fig. 13.

Time dependent results for the first alternative for test phase IV (power ramp at constant steam and argon mass flow rates) are shown in Fig. 14. Temperature increase is rather small in the beginning of the transient. A faster temperature increase begins at level 13 at about 4280 s. It may be due to a moderate escalation. A maximum temperature of 2150 K, i.e. about clad melting temperature, is reached at t = 4579 s, hence nearly 10 min after the beginning of test phase IV. Axial profiles at times when a maximum temperature of 2100 K in the bundle is reached are shown in Fig. 15.

Time dependent results for the second alternative for test phase IV, (steam mass flow reduction at constant electrical power input) are shown in Fig. 16. The faster temperature increase at level 13 at about 4000 s may be due to a moderate escalation similar to the faster temperature increase in the previous calculation. A second faster temperature increase is calculated at level 12 (elevation 0.85 m) at about 4070 s. A maximum temperature of 2150 K is reached at t = 4160 s, i.e. only 2.5 min after the beginning of phase IV. Axial profiles at times when a maximum bundle temperature of 2100 K is reached are shown in Fig. 17. Steam consumption is somewhat more pronounced than documented in the previous plots.

The axial temperature profiles in these two cases are rather similar to one another for the same maximum temperature. However, temperature increase is much faster in case of steam mass flow reduction. Therefore, temperature levels are generally higher in this case, and hence hydrogen production rate and oxide layer thickness are also higher.

Due to the fast temperature increase in case of steam mass flow reduction, the transient is very short and much faster than in the case of electrical power increase. Hence time for measurements as well as for operator intervention is very limited in the first case. The duration of the transient might be increased, when the electrical power is reduced at the time of steam mass flow reduction. This procedure had been proposed by UPM to avoid an undesired temperature escalation. This variant was not investigated in our calculations because such a test conduct is considered rather difficult to realize. In fact, an inappropriate change of electrical power might either jeopardize the integrity of the bundle or cool it down unintentionally; Fig. 8 demonstrates well the sensitivity of temperature with electrical power under similar conditions. Furthermore, the results of the CODEX B_4C test /1/ suggest that not much CH_4 formation can be expected for a steam mass flow of 1 g/s. For these reasons, a test conduct with a power transient instead of a steam mass flow reduction was favoured at FZK.

After inserting the geometry change, described above, into the S/R5 facility model a calculation for the whole test was made (Fig. 18). For the cool-down phase, the steam inlet temperature is set to 420 K for the whole test phase V. Cool-down is calculated to occur without temperature escalation (Fig. 19). This pre-test calculation was chosen as a basis for the experiment. As a basis to initiate cool-down, the bundle temperature in the hottest zone was used. In sum, the determination of the test conduct to be in accordance to all requirements was a tedious work.

3.3 Post-Test Calculations

Post-test calculations are based on the real test conduct as shown in Fig. 20 with the same modelling as for the pre-test calculations. Results are given in Fig. 21 – Fig. 23. Long-dashed lines refer to the 16f model. In the first transient, phase II, calculated temperatures are underestimated (Fig. 21), whereas during oxidation (phase III) a significant temperature increase is calculated which has not been measured (stabilized temperatures in the test). This leads to sensible deviations of calculated hydrogen production from measured values (Fig. 22). With the 32f model, results for phase II are not improved, but the agreement with the experiment for higher temperatures as in phase III is. Consequently, onset of temperature escalation is calculated to begin later, giving better agreement of oxide layer thickness and a smoother profile of linear electrical rod power at the time when the corner rod is withdrawn.

The difference of the results for the two axial discretizations is very pronounced for the oxide layer thickness and hydrogen production rate (Fig. 24), because for the fine axial discretiza-

tion an escalation is calculated just to have started, whereas for the coarse discretization it is calculated to begin about 120 s earlier. For this reason, the peak value of hydrogen production rate is calculated to be one order of magnitude larger for the coarse axial discretization. As can also be seen from Fig. 23 and Fig. 24, the fine axial discretization generally improves the agreement in the upper electrode zone. During cool-down, differences between experiment and calculation mainly seem to rise from different temperatures at the initiation of cool-down (Fig. 25). Improvement of results with increasing spatial resolution is well known and also found for calculations on QUENCH tests /7/. A further decrease of the mesh cell lengths would probably still improve the results somewhat, but the computational effort also increases drastically and is perhaps not justified at the moment, because code improvements are also being done and should be available before further calculations are performed.

Comparison of measured temperatures in the upper half of the heated zone suggests that especially at level 11 (elevation 0.75 m) physical or chemical processes occur, which are not yet understood. Probably this observation is not the main reason for all discrepancies. Comparison of test QUENCH-07 with QUENCH-09 shows that the experimental results for both tests differ substantially after the failure of the absorber rod, though in that phase the experimental conditions differ only marginally, if any. Further code development should therefore be postponed, until the reasons for the experimental differences are understood.

Calculations for test QUENCH-09, performed meanwhile /11/, suggest that a decrease of thermal conductivity of the shroud insulation material might improve the agreement in phase II. This item needs some more work to be done, because it is an aim of the analytical support at FZK to perform the calculations for all QUENCH tests with the same modelling. No further computational investigation of that sort is intended presently, because, besides to the open questions about the experiments, mentioned above, the oxidation model in S/R5 is being improved according to suggestions made by G. Schanz, FZK, in the COLOSS project.

Instead of using Cathcart and Urbanic-Heidrick correlations for low and high temperatures, respectively, as is standard in S/R5, the Leistikow and Prater-Courtright correlations with an interpolation between them are applied. In discussions during COLOSS meetings, it was pointed out, that it is necessary to include a steam supply limitation in the code, when the new oxidation model is applied. For the calculations presented here, the steam limitation model is used, as it is already implemented in the standard version of S/R5 /5/. It is also used for the calculations with the standard oxidation model, presented here. It is based on an analogy of heat and mass transfer and, because dimensionless numbers are used, it should essentially be applicable irrespective of the oxidation model. First results with this oxidation model suggest that the calculated hydrogen production agrees somewhat better with experimental data for lower temperatures, whereas in the high temperature regime a large overestimation is calculated. However, error checks for the new oxidation model are not yet finished.

3.4 Conclusions

The test conduct was originally planned to be similar to the planned in-pile test PHEBUS FPT3. Pre-test calculations with in-house version SCDAP/RELAP5 mod 3.2 show, however, that in the QUENCH facility the various aims of the test cannot be fulfilled at the same time. Especially the projected low steam flow phase at high bundle temperatures turned out to jeopardize the integrity of the QUENCH facility. Out of the variants for the final test protocol, proposed on the basis of such calculations, a power transient to reach very high temperatures in

the bundle before final cool-down is considered advantageous in comparison to a steam flow reduction. Post-test calculations show deviations to measured temperatures in the first transient already. Therefore, further investigations are necessary. Besides, a better understanding of experimental results is necessary, especially in view of the very different outcome of test QUENCH-09. For the second reason, further computational work and code development for B_4C absorber rods are not done actually, except that the Zry oxidation model in the code is being improved. The present computational results also show the necessity of a sufficiently fine spatial resolution of the computational domain.

4 PSI Calculations

Jon Birchley
Paul Scherrer Institut
Villigen

4.1 Strategy for experiment conduct

According to the final test protocol, the QUENCH-07 experiment should be conducted in five phases:

1. Initial stabilisation of energy balance and temperatures;
2. Power/temperature ramp to attain conditions relevant to absorber rod degradation and B4C oxidation;
3. Temperature plateau at ca. 1800 K of duration 15-20 minutes;
4. Temperature escalation to Zircaloy melting and early stage of fuel degradation;
5. Cool-down in steam.

Preliminary analyses demonstrated that attainment and stabilising of the target conditions are a significant challenge to the experimental team, mainly because the oxidation heat becomes a major contributor to the total heat production at temperatures above about 1700 K. Therefore, any departure from the planned conditions or any local hot spot can result in an uncontrollable temperature increase. A low steam flow might be used to limit the potential oxidation heat, but such a low flow also implies a low heat transfer to the fluid, again making it difficult to control the temperature. In order to achieve a temperature plateau it is necessary to balance the heat generation (electrical plus oxidation) with the heat removal (convection to the flowing stream plus radiation to the shroud). Because of these considerations, the following strategy for conducting the experiment is chosen:

1. Initialise the experiment at a moderate electrical power (3.8 kW total) and flow of 3 g/s steam plus 3 g/s argon at an inlet temperature of 620 K; the steam and argon flows are kept constant until the cool-down phase.
2. Increase the electrical power to achieve a rise rate of cladding temperature of not more than 0.4 K/s. This is done by ramping the heat input at a rate of 6 W/s, reducing the ramp rate to 4 W/s as the temperature rise rate approaches the target of 0.4 K/s and then keeping the power steady. This allows the target temperature of ca. 1800 K to be reached by the combined action of electrical and oxidation heat.
3. Apply a series of power increments as the temperature levels off or begins to decrease, to offset the reduction in oxidation rate as the oxide layer becomes thicker. In this way, the combined heat input remains almost constant, and in balance with the heat removal at ca. 1800 K. Maintain this temperature plateau for about 1000 s.
4. Apply a second power ramp of 6 K/s starting at the end of phase III, and continuing until a maximum temperature of 2300 K is reached.

5. Reduce the power to 4 kW and increase the steam flow to 15 g/s at an inlet temperature of 420 K to affect the cool-down.

4.2 Pre-Test Calculations for Final Test Protocol

4.2.1 Summary of calculations

The calculations have been done with PSI in-house version of S/R5 mod 3.2. Some differences to FZK in-house versions were kept intentionally, as will be explained later.

As explained above, achievement of the desired temperature history is a challenging task, and it is prudent to perform independent calculations to provide, hopefully, additional confidence that the strategy for test conduct will be effective, and to identify possible problems not apparent from a single calculation. The calculations performed by PSI are based on information on the QUENCH facility and planned test conduct according to the final test protocol, but using a version of SCDAP/RELAP5 and QUENCH input deck slightly different from those used by FZK. In particular, the PSI code version is essentially the same as the standard release MOD3.2/hx, but with the diffusion limit on the oxidation model modified to take account of the reduced partial pressure as the steam is consumed. By avoiding the same versions, it was intended to highlight any important sensitivity to input or code model uncertainties that might prompt reconsideration of the test conduct. The main results of two calculations by PSI are compared with the FZK calculation in Table 2.

4.2.2 Baseline calculation – case q07v16p1

As a preliminary, a checkout was performed by PSI using the same input as used by FZK. The case run shows similar qualitative behaviour, but somewhat lower temperatures and appreciably less oxidation of the Zircaloy cladding. Closer investigation shows that the difference is not connected with the modification of the oxidation model, but instead follows on from a slower temperature rise in the bundle which is noticeable already before the onset of oxidation. This is traced to a modification in the FZK code version to correct errors in the radiation heat transfer. Although direct effect of the model change was not large, the temperature difference becomes magnified via the positive feedback on Zircaloy oxidation. Since computational uncertainties are unavoidable, it is useful to include this variation in radiation model to assess the potential impact of such an uncertainty.

The first main PSI prediction calculation was performed using a slightly modified input deck which allowed maximum ballooning of 2 percent and an artificial treatment of the four corner rods to circumvent a code error that is manifest when melting occurs for rods composed of nearly solid Zircaloy. Despite some concern that due to the sensitivity of the transient, these changes might affect prediction of the temperature plateau, there was no noticeable difference due to the input model change up to and including the plateau phase. The checkout case is therefore not discussed further.

The results of the baseline case are shown in figures Fig. 26 to Fig. 30. The temperature rise rate increases due to the power ramp, reaching a maximum of slightly less than 0.4 K/s at 2000 s. The bundle power history shows the contributions from electrical and oxidation heat. Although the electrical power is the same as in the FZK calculation, the oxidation rate is lower during the important phase when the temperature plateau is being reached, and hence the temperatures are lower by about 100 K and with a small residual rise rate as the electrical power is stepped up. The temperatures increase again during the second power ramp,

starting at 4000 s, until the cool-down is initiated when a temperature of 2300 K is reached at 4750 s. The increased steam flow and reduction in electrical power then affect a rapid cool-down. The hydrogen generation rate generally follows the temperature escalation and reaches a peak of 85 mg/s, corresponding to 0.95 g/s rate of steam consumption – i.e. slightly less than one-third of the original steam inlet flow. Since the oxidation is far removed from steam starvation, any further escalation following the power reduction and increase in flow rate would be unlikely. Although the temperature for initiation of cool-down is fixed at 2300 K, the final mass of hydrogen generated and maximum thickness of the oxide layer, 47 g and 630 µm respectively, are less than predicted by FZK using their code version. Concerning the oxide thickness, it is noted that the code output contains incorrect values for the oxide thickness, though the calculation itself seems to be correct. If the cladding is not completely oxidised the code outputs the depth of Zircaloy which has been oxidised, and not the oxide thickness itself. The output value then jumps to the (apparently) correct value when the cladding is 100 percent oxidised. In the case of QUENCH, the values are approximately 750 µm and 1050 µm.

4.2.3 Modified power history – case q07v16p22

From the point of view of experiment conduct, it is worthwhile to assess to what extent the operating conditions might need to be changed to achieve a temperature plateau at about 1800 K at the hottest location, given that the PSI baseline calculation predicted temperatures lower by about 100 K. We consider, then, the following questions. Can a temperature plateau within an uncertainty range of 1700 – 1800 K be regarded as acceptable? Is it possible to control the operating conditions so as to achieve 1800 K?

One possibility is to continue the first power ramp for a longer period and then continue at a correspondingly higher power history. Trial calculations were performed in an attempt to match the temperatures at the end of the first power ramp with those predicted by FZK, and then continue with a constant power phase followed by a series of power steps. However, continuing the power ramp carries the risk that it might set in train a premature oxidation transient even though the power ramp is terminated at temperatures well below 1800 K. A first trial calculation (not shown) was performed in which the power ramp is continued until a temperature of 1430 K and a rise rate of 0.45 K/s. In this case, the temperature continues to rise at an increasing rate, without achieving a plateau.

Results of a second calculation are shown in figures Fig. 31 to Fig. 35. The power ramp is continued for just a further 125 s beyond the baseline case, until the rise rate is 0.39 K/s, effectively the same as in the FZK calculation, and then kept constant until the first power step, after which it again follows the baseline power history. As a result, a slightly higher temperature is reached during phase 2. A temperature of 1800 K at the hottest location is achieved at the start of phase 3, with very stable temperature throughout the plateau as the power steps just offset the reduction in oxidation heat. The second power ramp starting at 4000 s results in an escalation to 2300 K, as before. The final mass of hydrogen, 56 g, is close to the FZK result. The maximum thickness of Zircaloy oxidised is 715 µm which corresponds to about 95 percent oxidation, compared with 100 percent predicted by FZK.

4.2.4 Discussion of results

The PSI calculations exhibit similar temperature and oxidation history and confirm the prediction by FZK. The results indicate that a temperature plateau of 1700 to 1800 K can be achieved for 15-20 minutes, provided the power history is carefully controlled.

A critical phase is the first power ramp, which should be terminated before the temperatures increase too rapidly; the calculations indicate a rise rate of 0.4 K/s as a suitable criterion to terminate the power ramp, which will allow the rise rate to slow down to almost zero and hence provide a smooth transition to the temperature plateau. The power can then be incremented as necessary if the temperatures decrease during the plateau. Despite the good expectation based on the calculated results, some uncertainty remains. Quite a modest difference in the code versions results in a change in plateau temperature of about 100 K. It should be noted that in the FZK and PSI variant case the temperature plateau remains only slightly below 1853 K, the temperature at which the code model exhibits a cliff-edge change to faster kinetics. Although the model is a simplification of the kinetics, it is known that the oxidation rate increases sharply at about 1850 K. A temperature of more than 1800 K would therefore leave rather a small margin against the risk of a premature excursion.

About 60 g hydrogen is expected, with a rapid generation rate during the final escalation but with the most of the mass generated during phase 3. Most of the Zircaloy will experience fairly shallow oxidation, except in the hottest locations near the top of the heated length where complete or nearly complete oxidation is expected. Finally, the calculations indicate no risk of a further escalation during the cool-down.

5 UPM Calculations

José Antonio Fernández Benítez
Mercedes Ortega Bernardo
Universidad Politécnica de Madrid

The work is related to pre-test calculations according to the final test protocol. As a computational tool, the code ICARE2 V3mod1 is used.

5.1 Case 0

This case is executed following the new features of the final test protocol, although it presents a variation concerning the temperature escalation stage (phase III). It could be obtained by reducing both the coolant flow rate and the electric power level, in order to compensate the rapid thermal response of the bundle.

Effectively, the only reduction of the steam flow (from 3 to 1 g/s) leads to a rapid degradation of the bundle (in a couple of minutes). This situation could be balanced by reducing the power level from 12 to 8 kW, approximately, which results in the slower progression of the damage with a total duration of 10 minutes (top of Fig. 36).

The thermal response shows a good agreement with the desired one. The total hydrogen production is evaluated over 50 g, but only a few per cent (less than 2 g) are due to control material oxidation (bottom of Fig. 36 to Fig. 37).

5.2 Cases 1 and 2

Because of the strong sensitivity of bundle temperatures to the electric power delivered, the action of reducing the power level in the beginning of Phase III seems to be not recommended, since an inappropriate value of this (and the design window is very thin) could lead to undesirable situations, like cool-down in one direction, or loss of integrity in the opposite. In addition, and based on experimental practice, this actuation could be difficult to perform.

Therefore, a new alternative is proposed which consists of the bundle temperature control by means of the electric power regulation instead of the reduction of the coolant flow rate (lesson derived from the COLOSS Topical Meeting on QUENCH-07 /4/).

Two different cases (called case 1 and 2) have been simulated. In case 1 the bundle heating rate is moderate (0.2-0.25 K per second) due to a constant power ramp of 3 W/s. On the other hand, a 6 W/s power ramp is forced in case 2 which leads to a higher bundle temperature increasing rate (max 0.45 K/s), Fig. 40.

In both cases, three different stages are clearly defined (phases II, II, and IV according to the final test protocol). First stage (phase II) is longer in case 1, 14 min versus 10 min, due to the different bundle heating velocity. The following stages are of similar duration, although the oxidation stage (phase III) is carried out in different way from one case to another (steps versus ramp). That is the reason why a higher value of maximum temperature is reached in case 2 (1835 K versus 1805 K). Temperature escalation stage (phase IV) is reached in both cases by increasing the electric power at a constant value of 6 W/s until a maximum cladding temperature of 2300 K is obtained (Fig. 38).

5.2.1 Thermal response

The evolution of the bundle temperature at different levels is quite similar in both cases, and satisfies the requirements of the final test protocol (Fig. 39).

The regulation of temperature is a critical point in the test performance. The level of 1800 K is critical for Zircaloy oxidation (due to the changes in the configuration and, also, in the kinetics) and therefore an uncontrolled chemical power released due to oxidation could lead to a temperature escalation. In addition, maintaining the maximum temperature in the range of 1800-1900 K is also hard to reach. The Zr oxidation process slows down as Zr is consumed and temperatures are unchanged (see evolution of hydrogen generation rate). In order to maintain the plateau of temperature, more energy must be supplied in the bundle which leads to increase the electric power (by means of little steps in the case 1 or by a smooth ramp in the case 2).

Anyway, Fig. 44 illustrates the strong sensitivity of the bundle to the electric power. The different temperature evolutions are obtained with little variations in the power level (ramps of 0.6 to 0.8 W/s; steps of 500 W; 50 s in advance or delay...). See that even one of the executions results in a non-controlled temperature excursion.

5.2.2 Oxidation

The duration of phase III depends on the oxide layer thickness to be reached, since no starvation conditions are going to be reached (no steam reduction is estimated as originally). According to our calculations with ICARE2 a 15 minutes stage leads to maximum ZrO_2 thickness of 400 μm (390 and 382 μm in cases 1 and 2, respectively). This value was considered as optimum by the experimentalists (Fig. 41).

5.2.3 Final aspect of the bundle

The final state of the control rods at higher elevations is rather different from one at lower elevations. Whereas at the bundle top the original configuration has almost disappeared, at middle and lower elevations the damage is negligible. This is due to the temperature reached at the middle-bottom part (0-50 cm), not high enough to result in eutectic reactions between B_4C and SS. Only little amounts of eutectic mixture coming from upper elevations are relocated in the middle zone.

Above 60 cm, this eutectic reaction becomes evident. It starts to occur at the end of phase II. From 75 to 100 cm the original geometry is lost, and so, the protective capability of the guide tube. The remaining uncladded B_4C is, then, susceptible for oxidation. Above 90 cm, even the control material has also disappeared.

5.2.4 Hydrogen generation

Concerning the hydrogen production, the total amount of H_2 released due to oxidation processes is in the range of 60-70 g. Both calculations are in good agreement in relation to the total H_2 released in the beginning of the phase IV (approximately, 40 g; generation rate between 15-25 mg/s). Nevertheless, the peak of H_2 generation rate corresponding to the temperature escalation is somewhat different from one case to another (120 mg/s versus 90 mg/s). The exact value of the maximum temperature reached (not coincident in both cases) could justify this divergence. This final increment is the reason for the different total amounts of hydrogen produced (Fig. 42).

Only a 3-4% of the total H_2 produced is due to oxidation of control rod material. In particular, approximately 2 g are obtained. As mentioned previously, the final excursion in the H_2 generated leads to a little variation range (1.9-2.2 g). Keep in mind that control material oxidation is only possible if B_4C pellets get in touch with steam, which requires the loss of the integrity of the protection layer of SS (cladding) and Zircaloy (tube guide). This situation occurs during the phase II and justifies the delay observed between the Zircaloy-oxidation and B_4C-oxidation (Fig. 43).

NOTE: The results concerning hydrogen production due to oxidation of control rod material are obtained with the simple model existing in ICARE2, and their validity is precisely a goal of future developments.

5.3 Conclusion

The main conclusion of this set of calculations concerns the extreme sensitivity to some parameters, in particular, the electric power. It results in a very small design window, and therefore a closely fitted test conduct is required for success.

6 General Conclusions

Computational analysis has been done before and after the test QUENCH-07. The present report demonstrates the status of at least part of this work at the end of the COLOSS project in the Fifth Framework Programme on Nuclear Fission Safety, launched by the European Community.

Since test QUENCH-07 differed in more than one aspect from previous tests in the QUENCH facility at FZK, more attention than usual had to be paid to define the test conduct. To reduce the uncertainties, always related to pre-test calculations, this work was performed independently by several institutions, participating in the COLOSS project, and with different code systems, currently used for safety analyses in nuclear power reactors.

All participants calculated the same trends of results. In particular, they predicted that due to the elevated temperatures to be maintained for a long time the QUENCH facility would be rather sensitive to changes of experimental parameters as electrical power input and that the facility might even be damaged during the test. This sensitivity is still enhanced, when the steam mass flow is reduced, because the lower conductive heat removal is decreased. Therefore, the large computational effort was necessary to define an appropriate test conduct. The comparison of experimental data of this and the subsequent test, QUENCH-09, justified this work and the insight gained during its course.

7 Acknowledgement

The test QUENCH-07 and the related computational support were co-financed by the European Community under the Euratom Fifth Framework Programme on Nuclear Fission Safety 1998 – 2002 (COLOSS Project, contract No. FIKS-CT-1999-00002).

8 Literature

/1/ Hozer, Z., Nagy, I., Windberg, P., Balasko, M., Matus, L., Prokopiev, O., Czitrovszky, A., Nagy, A., Jani, P.: CODEX-B4C Experimental Data Report, SAM-COLOSS-P020, D17, Budapest, Oct. 2001.

/2/ Steinbrück, M., Homann, C., Miassoedov, A., Schanz, G., Sepold, L. Stegmaier, U., Steiner, H.: Results of the B_4C Control Rod Test QUENCH-07, FZKA 6746, to be published.

/3/ Sepold, L., Krauss, W., Miassoedov, A., Steinbrück, M., Stuckert, J.: QUENCH-09 Quick Look Report, SAM-COLOSS-P041, Karlsruhe, Nov. 2002.

/4/ Miassoedov, A: Minutes of the COLOSS Topical Meeting on QUENCH-07 Test, SAM-COLOSS-M006, Karlsruhe, Feb. 8, 2001.

/5/ The SCDAP/RELAP5 Development Team: SCDAP/RELAP5/MOD 3.2 Code Manual, NUREG/CR-6150, INEL-96/0422, Idaho Fall, Idaho, USA, 1997.

/6/ Hering, W., Homann, C.: Improvement of the Severe Accident Code SCDAP/RELAP5 mod 3.2 with respect to the FZK QUENCH facility, FZKA 6566, to be published.

/7/ Hering, W., Homann, Ch., Lamy, J.-S., Miassoedov, A., Schanz, G., Steinbrück, M., Sepold, L.: Comparison and Interpretation Report of the OECD International Standard Problem No. 45 Exercise (QUENCH-06), FZKA 6722, July 2002.

/8/ Sanchez, V., Elias, E., Homann, Ch., Hering, W., Struwe, D.: Development and Validation of a Transition Boiling Model for the RELAP5/MOD3 Reflood Simulation, FZKA 5954, Sep. 1997.

/9/ Hofmann, P., Hering, W., Homann, C., Leiling, W., Miassoedov, A., Piel, D., Schmidt, L., Sepold, L., Steinbrück, M.: QUENCH-01 Experimental and Calculational Results, FZKA 6100, Nov. 1998.

/10/ Hofmann, P., Homann, C., Leiling, W., Miassoedov, A., Piel, D., Schanz, G., Schmidt, L., Sepold, L., Steinbrück, M.: Experimental and Calculational Results of the experiments QUENCH-02 and QUENCH-03, FZKA 6295, July 2000.

/11/ Homann, Ch., Hering, W.: Analytical Support for B_4C Control Rod Test QUENCH-09, FZKA 6853, SAM-COLOSS-P057, to be published.

9 Tables

Table 1: Test conditions and results of first pre-test calculations

run	steam flow	argon flow	P_{red}	T_{red}	rupt strain	clad melting
	g/s	g/s	kW	K		
q07v01	0.4	3	-	-	0.18	+
q07v02	“	“	-	-	“	+
q07v03	“	“	19	2000	“	+
q07v04	“	“	18	1800	“	+
q07v05	“	“	17	1600	“	+
q07v06	“	“	12	1800	“	+
q07v07	“	“	5	1600	“	+
q07v08	0.5	“	“	“	“	+
q07v09	0.4	10	“	“	“	-
q07v09.1	“	6	“	“	“	+
q07v09.2	“	4	“	“	“	+
q07v09.3	“	5	“	“	“	+
q07v09.4	0.3	6	“	“	“	+
q07v09.5	“	8	“	“	“	-
q07v10	0.4	6	6	“	“	+
q07v11	“	“	7	“	“	+
q07v12	“	“	8	“	“	+
q07v13	0.3	8	5	“	0.05	-
q07v14	1.0	6	“	“	0.01	-
q07v14.1	1.0	4	“	“	“	-
q07v14.2	1.0	3	“	“	“	+
q07v15.0	1.0	6	5.5	“	“	-
q07v15	1.0	4	“	“	“	+

The table shows the test conditions during the low steam mass flow phase underlying pre-test calculations for the original and the modified test protocol. As a rough indication for the predictions the occurrence of clad is used.

P_{red} indicates the value to which power is reduced in the low steam flow phase; T_{red} is the maximum bundle temperature at the time of electrical power reduction. For run q07v01 double sided oxidation has been assumed.

Table 2: Comparison of PSI and FZK results at various times

Event/Parameter	FZK: q07v17	PSI: q07v16p1	PSI: q07v16p22
End of first power ramp (s)	**1585**	**1585**	**1710**
total electrical power (kW)	12.5	12.5	13.0
maximum temperature (K)	1244	1215	1265
rise rate (K/s)	0.40	0.36	0.39
H2 generation rate (mg/s)	5	3.1	4.0
H2 mass (g)	1.7	0.8	1.2
max depth of oxidised Zr (µm)	15	13	18
Start of plateau (s)	**3000**	**3000**	**3000**
total electrical power (kW)	12.8	12.8	13.1
max cladding temperature (K)	1778	1644	1770
rise rate (K/s)	0.24	0.17	0.25
H2 generation rate (mg/s)	22	13	20
H2 mass (g)	21	13	17
max depth of oxidised Zr (µm)	195	138	182
End of plateau	**4000**	**4000**	**4000**
total electrical power (kW)	14.0	14.0	14.0
max cladding temperature (K)	1842	1740	1780
rise rate (K/s)	0.04	0.06	-0.1
H2 generation rate (mg/s)	16	13	11
H2 mass (g)	41	26	34
max depth of oxidised Zr (µm)	394	271	368
Start of cool-down	**4600**	**4720**	**4882**
total electrical power (kW)	17.6	18.32	19.29
max cladding temperature (K)	2304	2300	2300
rise rate (K/s)	2.7	4.3	3.3
H2 generation rate (mg/s)	72	85	81
H2 mass (g)	57	42	52
max depth of oxidised Zr (µm)	689	540	640
End of experiment			
H2 mass (g)	60	46	56
max depth of oxidised Zr (µm)	1060	630	715

10 Figures

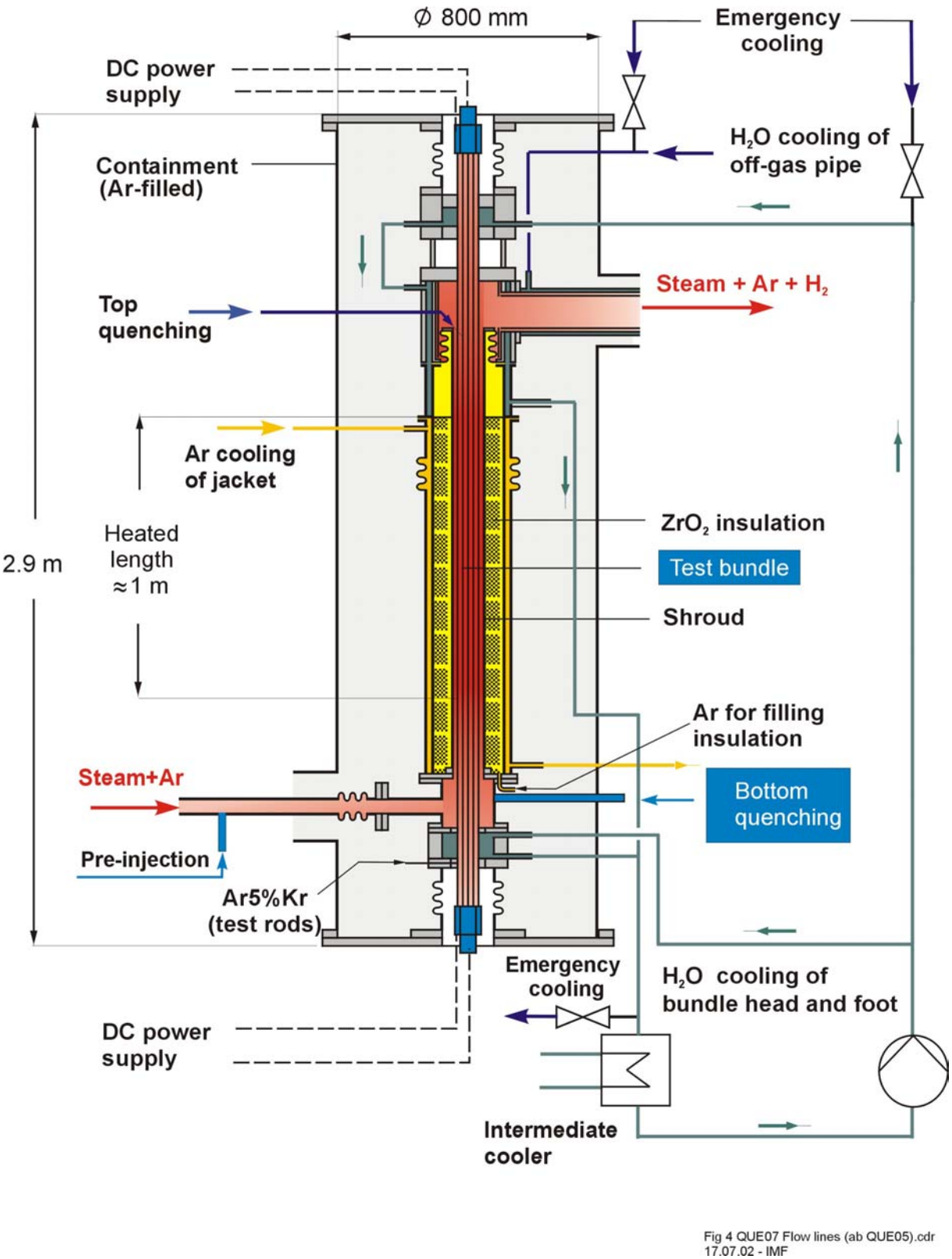

Fig. 1: Main flow paths in the QUENCH facility

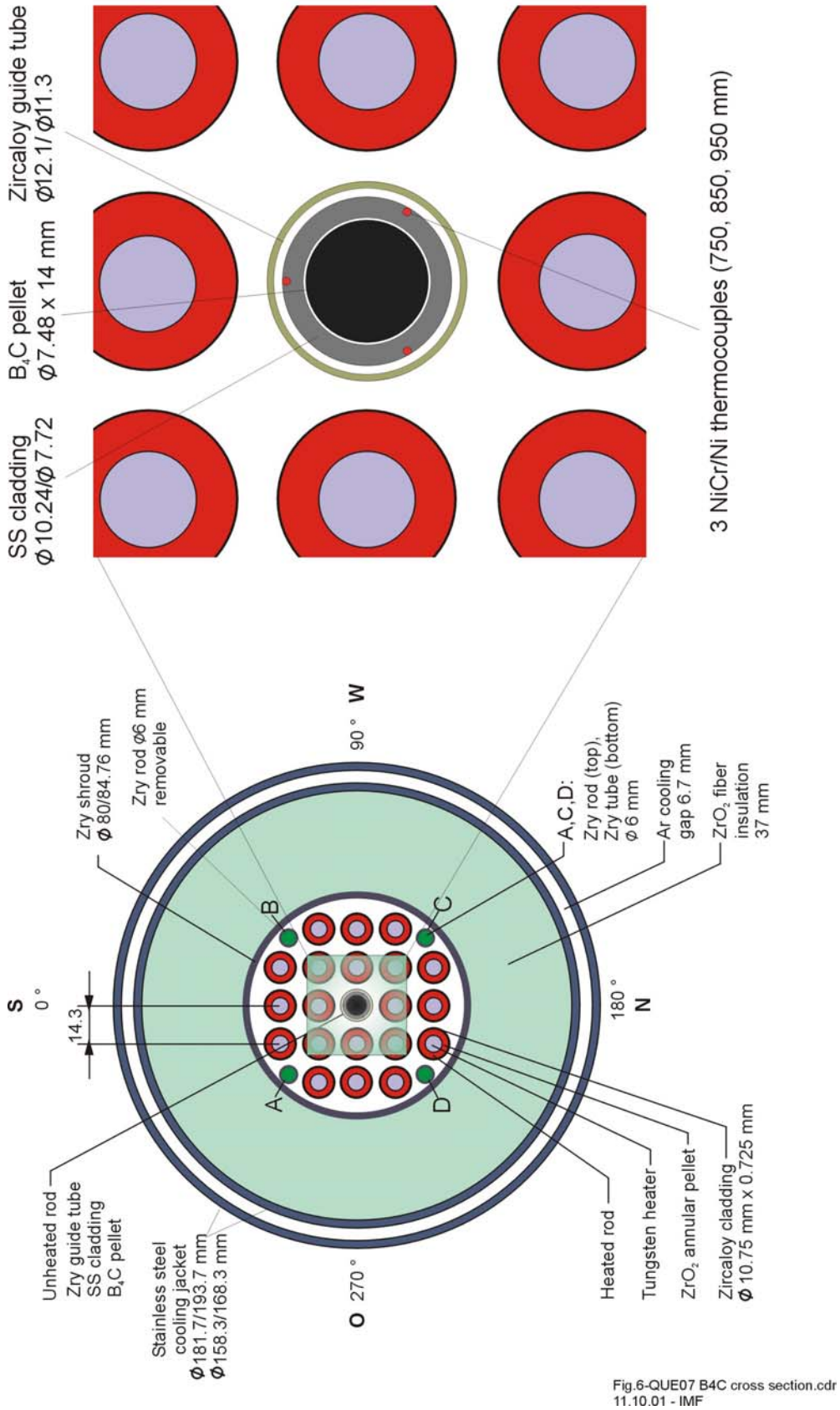

Fig. 2: Cross section of the test section for QUENCH-07

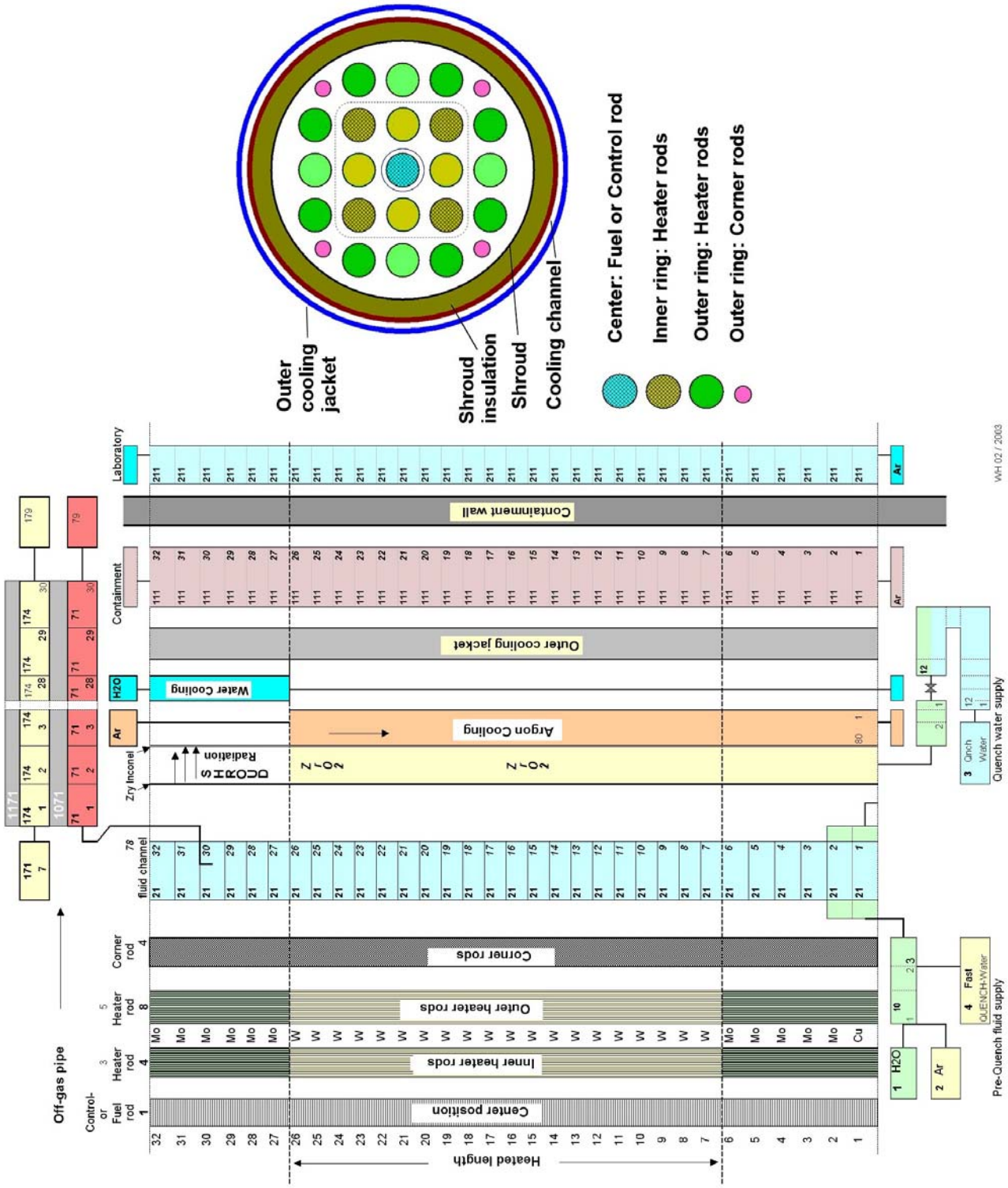

Fig. 3: Modelling of the QUENCH facility with SCDAP/RELAP5

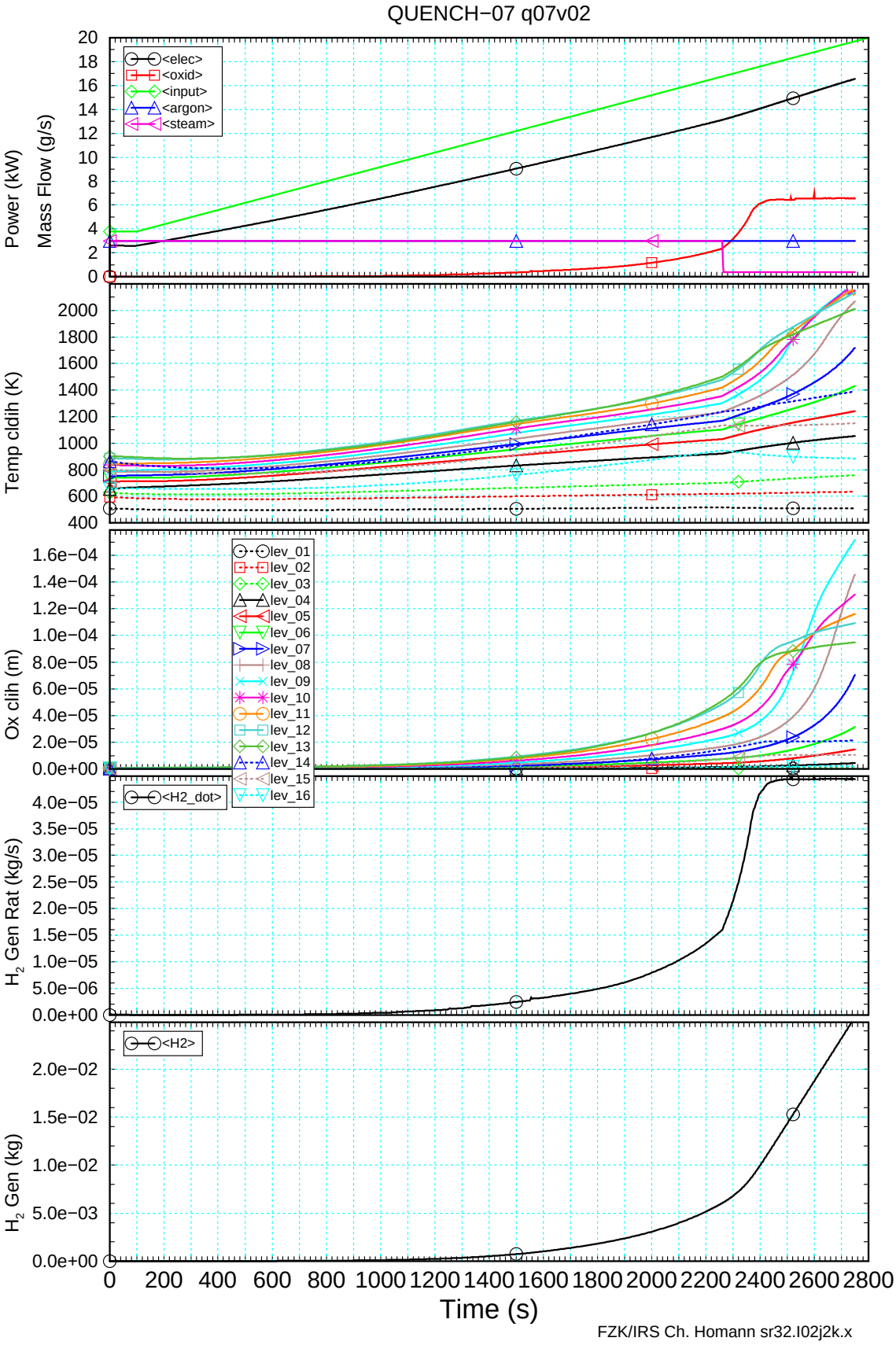

Fig. 4: FZK (OTP): selected variables as a function of time

The figures shows from top to bottom power and mass flow rates, clad surface temperature and oxide layer thickness of inner heated rods at the various axial levels, hydrogen production rate, and cumulated hydrogen mass.

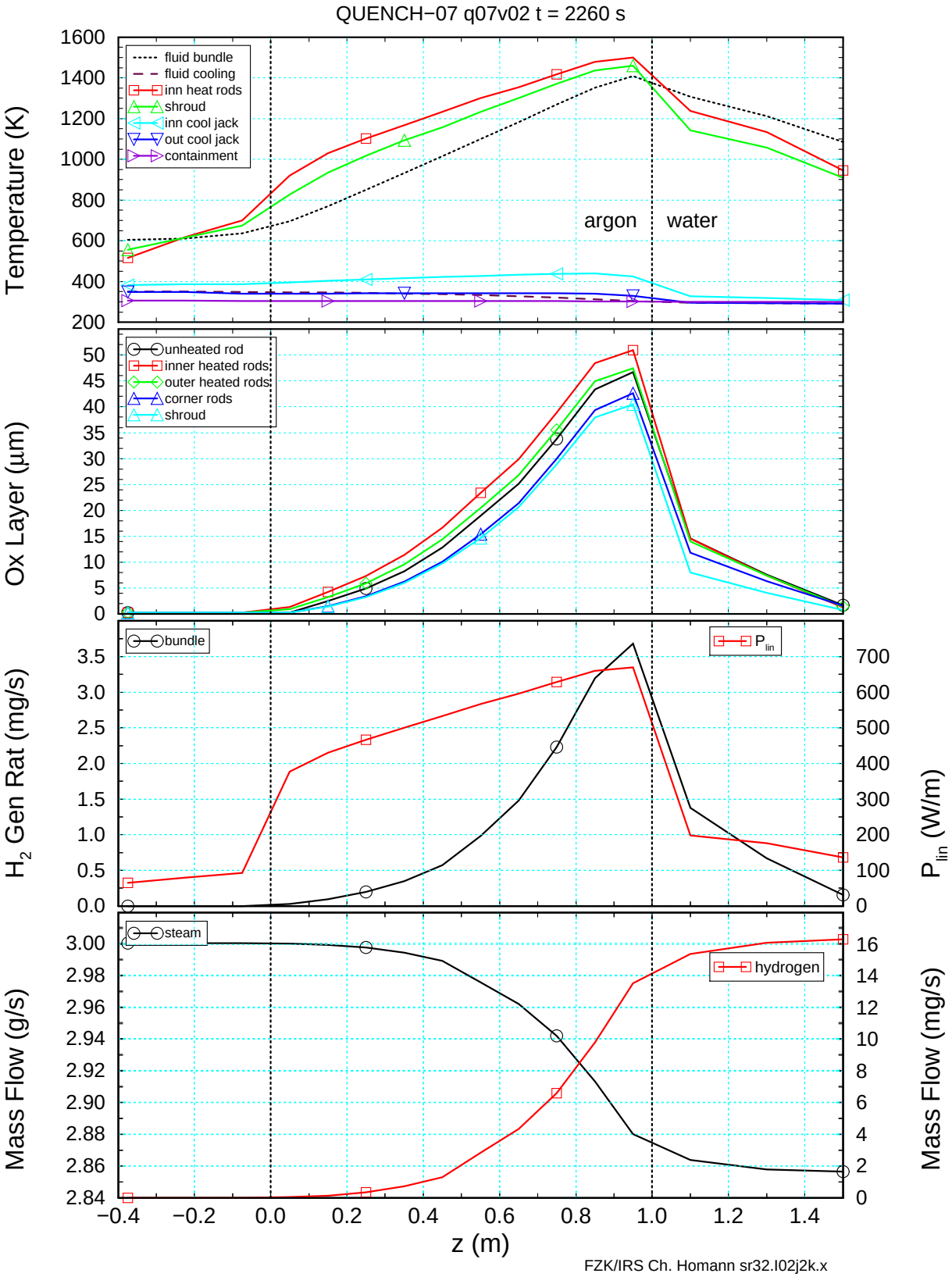

Fig. 5: FZK (OTP): axial profiles of selected variables at the time of steam flow reduction

The figures shows from top to bottom temperatures, oxide layer thickness, hydrogen production rate, linear electrical rod power, steam and hydrogen mass flow rates.

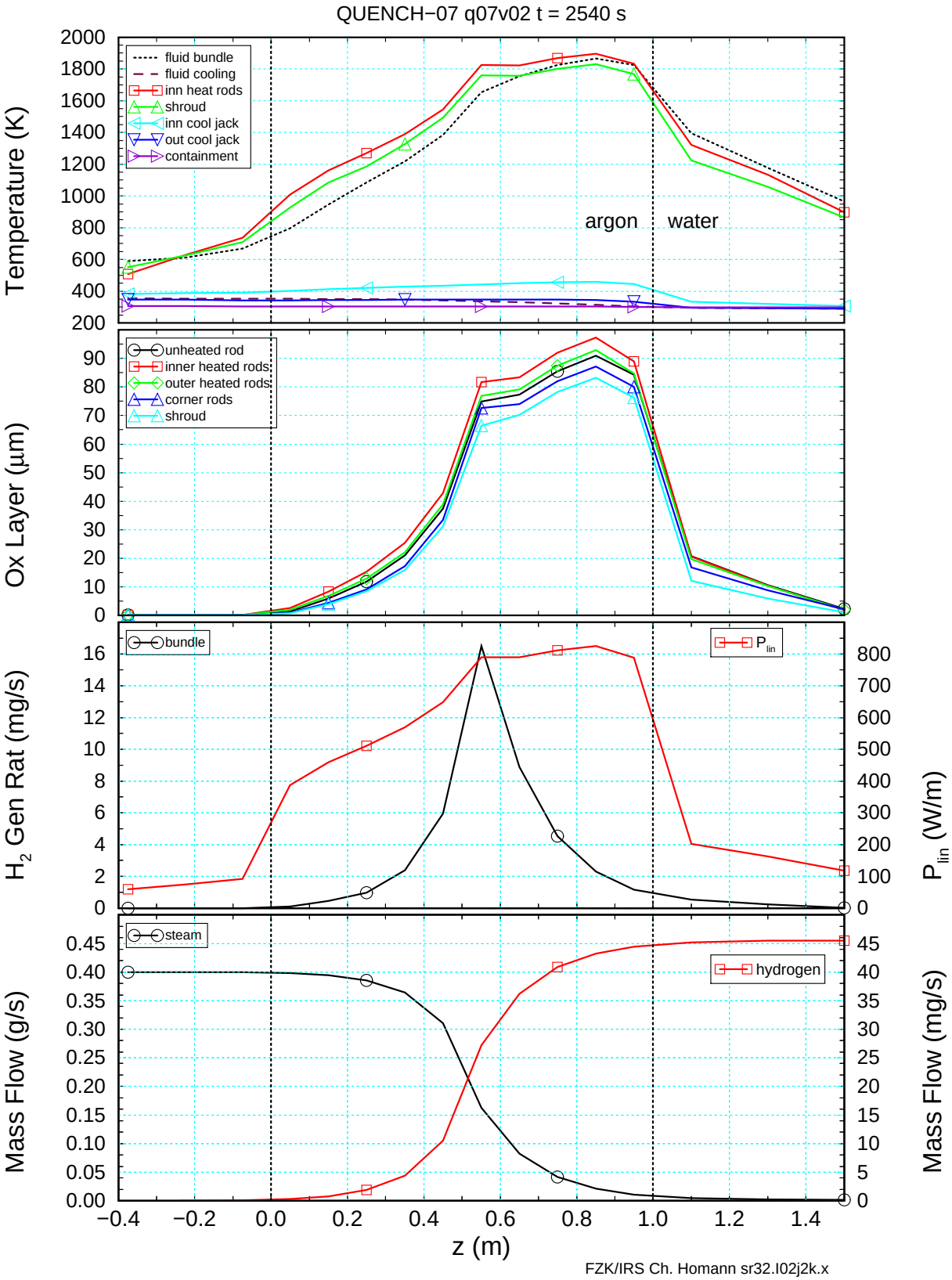

Fig. 6: FZK (OTP): axial profiles of selected variables at 2540 s

The figures shows from top to bottom temperatures, oxide layer thickness, hydrogen production rate, linear electrical rod power, steam and hydrogen mass flow rates.

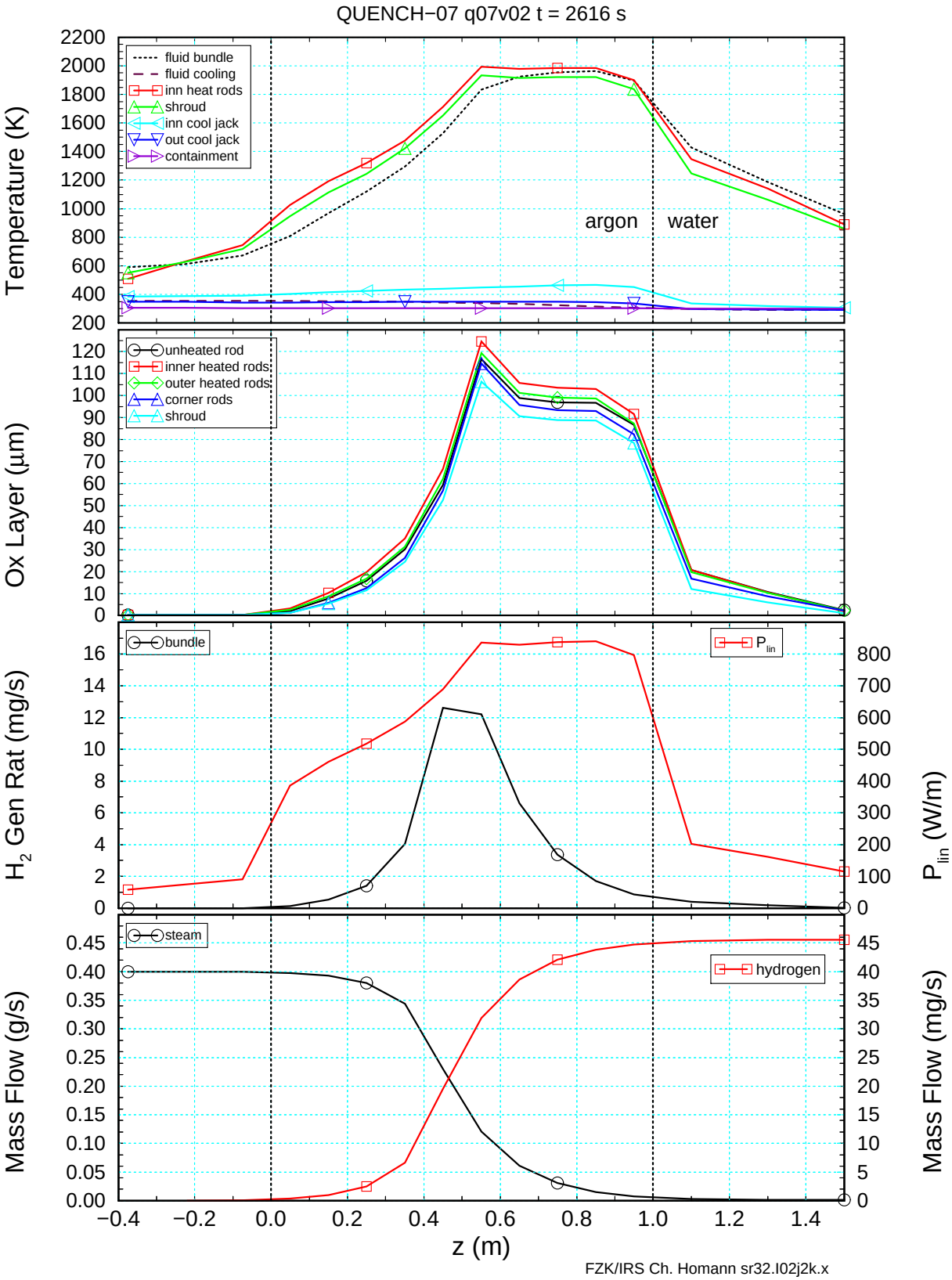

Fig. 7: FZK (OTP): axial profiles of selected variables at 2616 s

The figure shows from top to bottom temperatures, oxide layer thickness, hydrogen production rate, linear electrical rod power, steam and hydrogen mass flow rates.

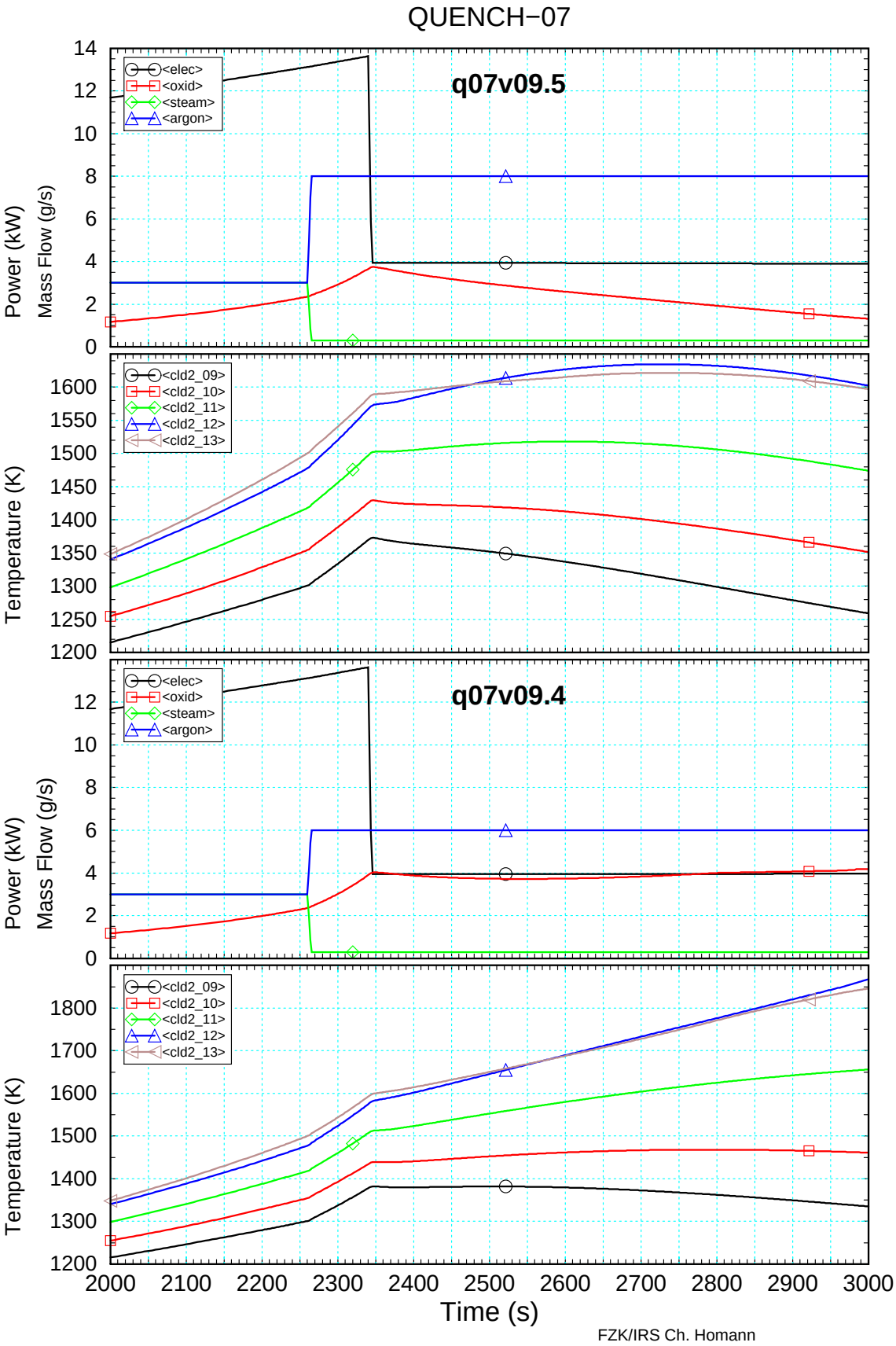

Fig. 8: FZK (MTP): selected variables for two different argon flow rates

The figure shows power, mass flow rates, and clad surface temperature of inner heated rods at axial levels 9 to 13 (elevations 0.55 to 0.95 m) for two different argon flow rates as a function of time.

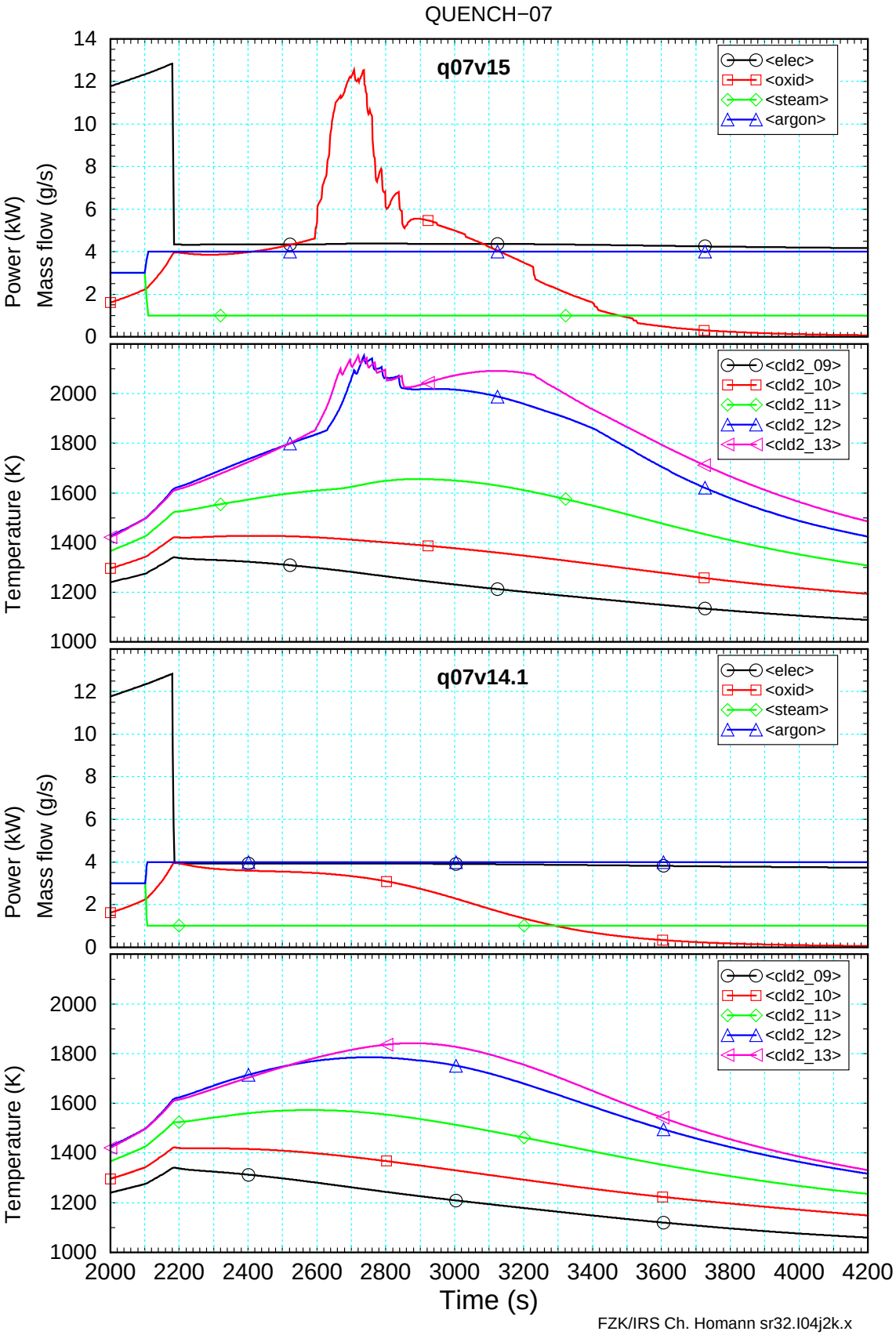

Fig. 9: FZK (MTP): selected variables for two different electrical powers

The figure shows power, mass flow rates, and clad surface temperature of inner heated rods at axial levels 9 to 13 (elevations 0.55 to 0.95 m) during low steam flow conditions for two different electrical powers during low steam flow conditions as a function of time.

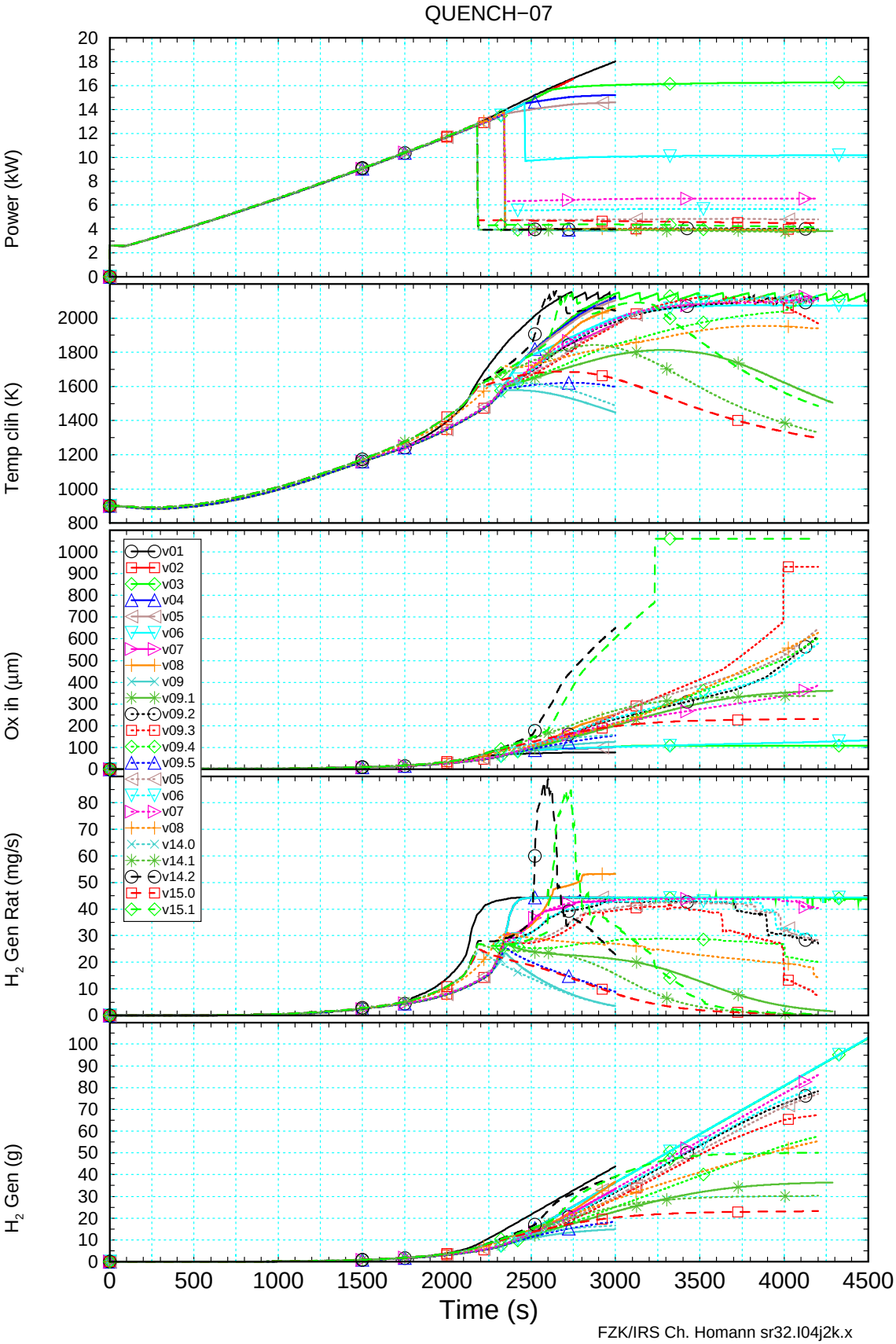

Fig. 10: FZK (OTP and MTP): survey of calculations

The figure shows from top to bottom electrical power release into the bundle, oxide layer thickness and clad temperature for the inner heated rods at axial level 13 (elevation 0.95 m), hydrogen production rate and cumulated hydrogen mass as a function of time.

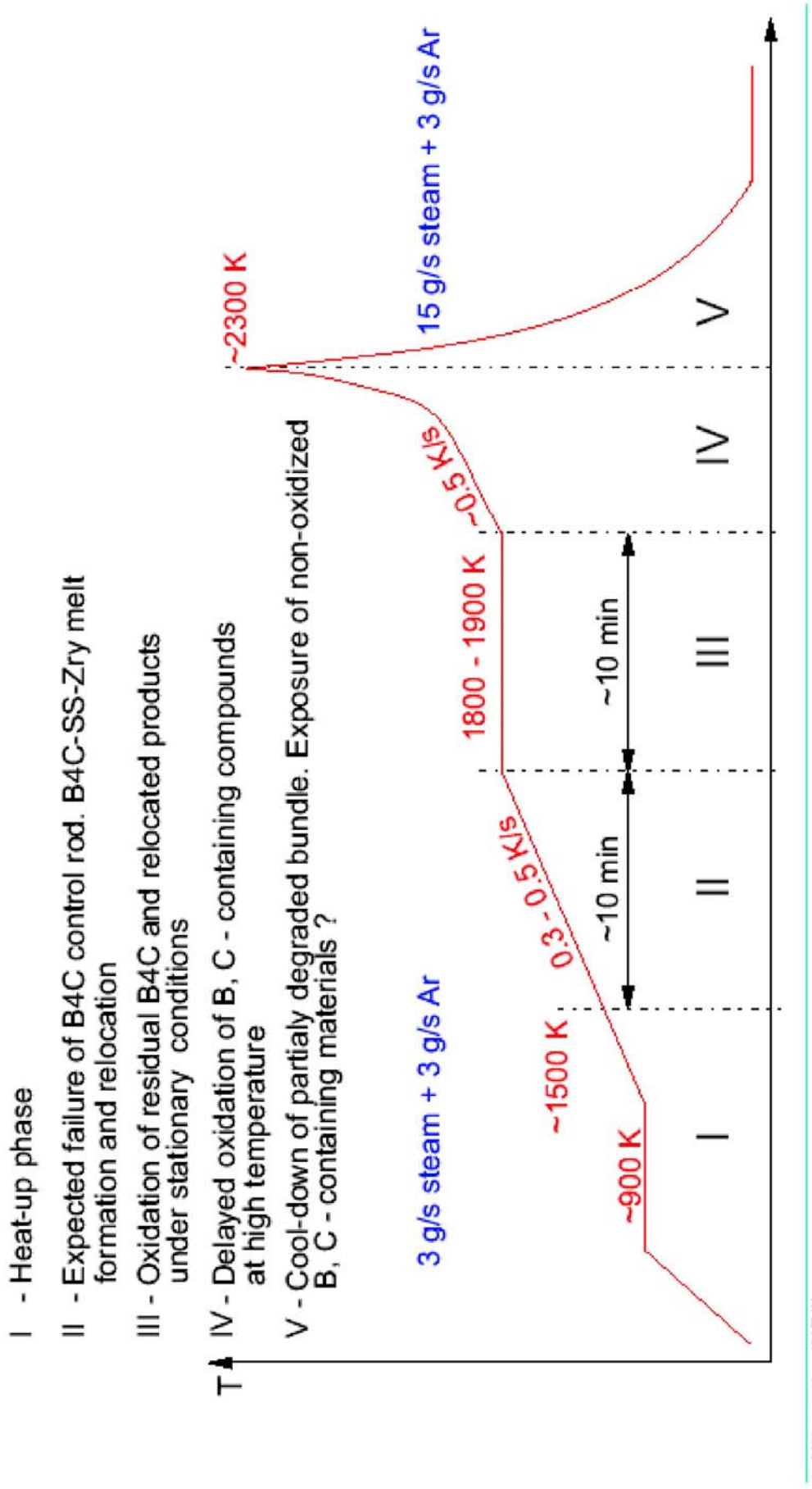

Fig. 11: Final test protocol for QUENCH-07

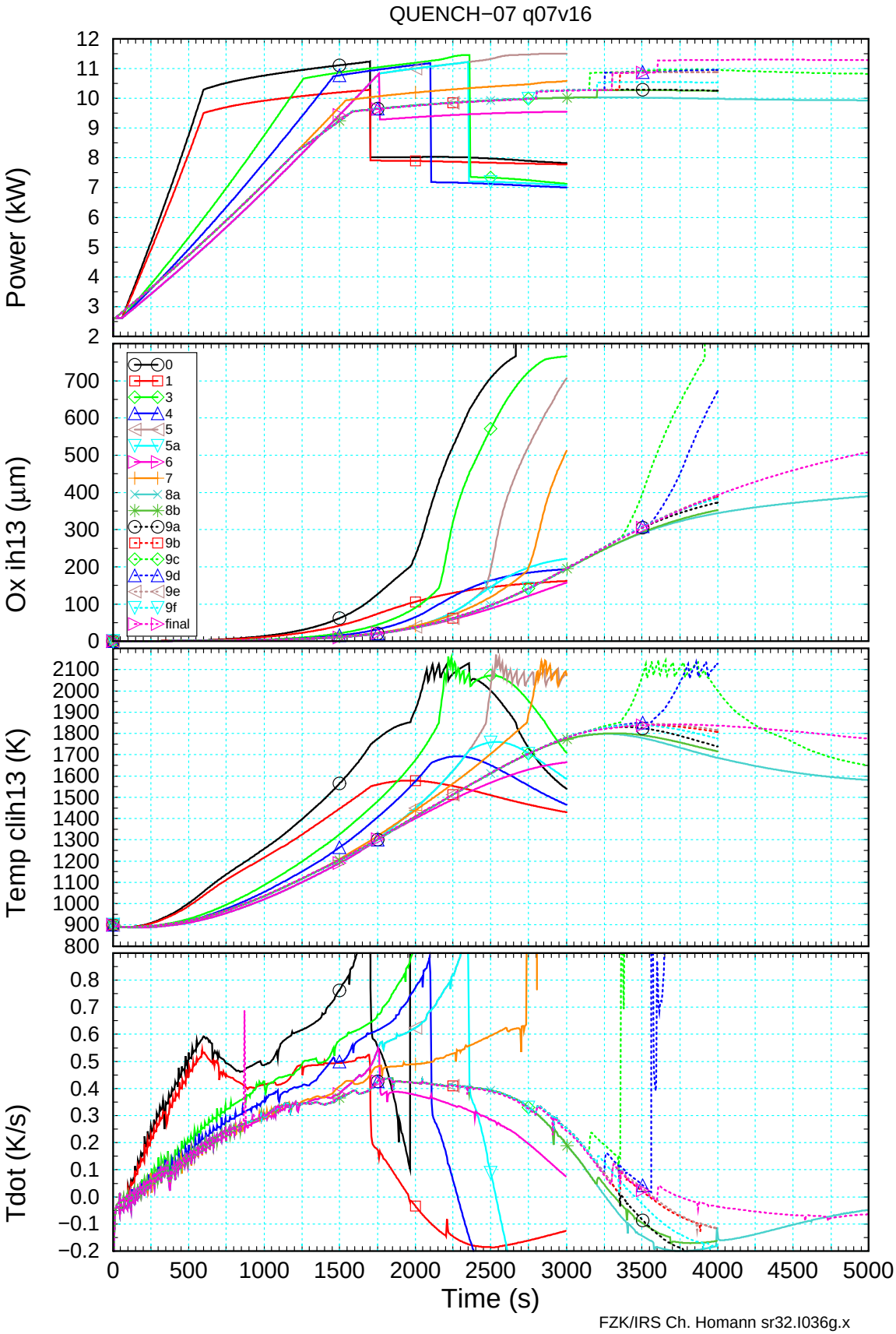

Fig. 12: FZK (FTP): survey of calculations

The figure shows from top to bottom electrical power release into the bundle, oxide layer thickness, clad temperature for the inner heated rods and its time derivative at axial level 13 (elevation 0.95 m) as a function of time.

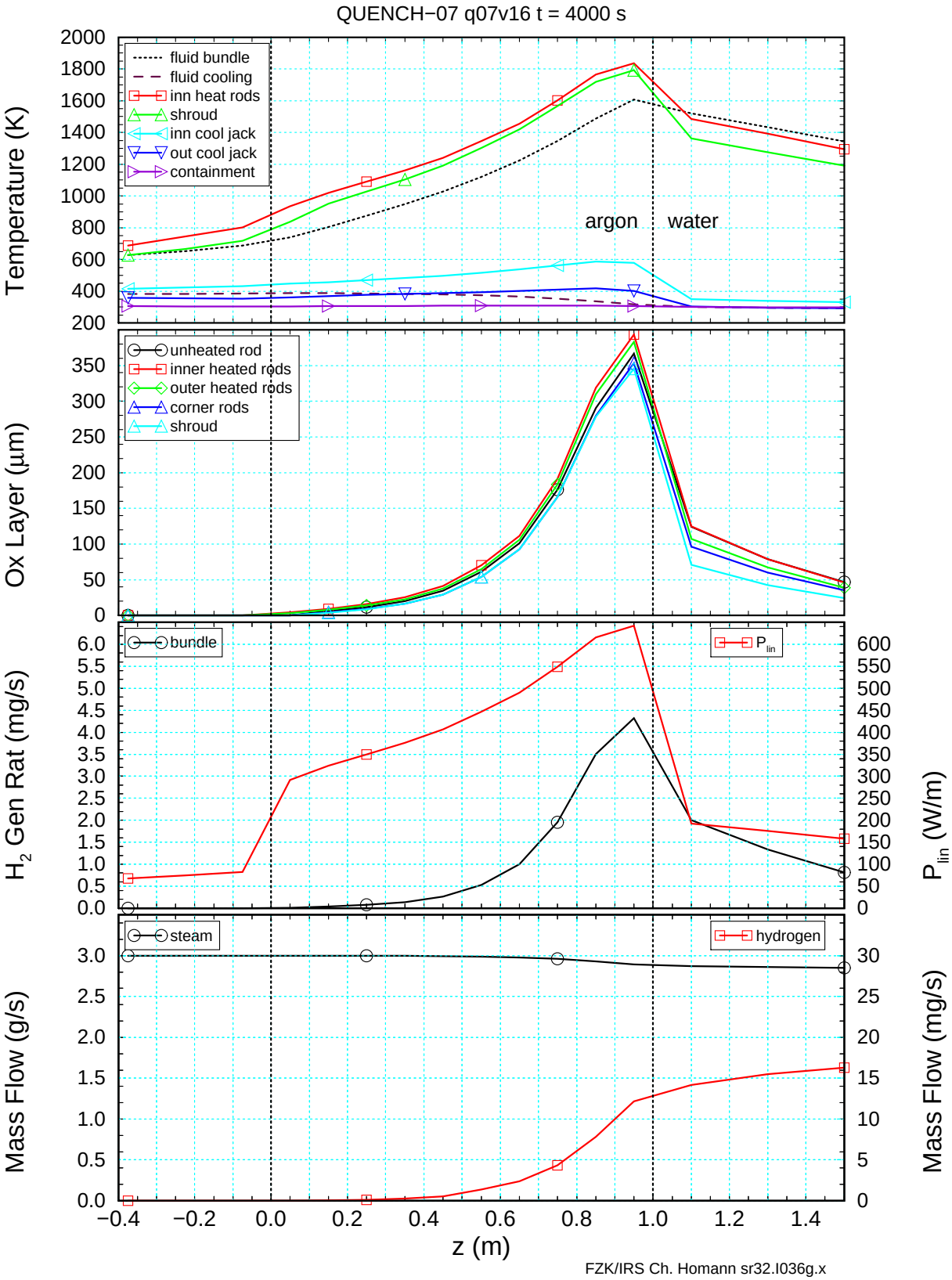

Fig. 13: FZK (FTP): axial profiles of selected variables at the end of test phase III

The figure shows from top to bottom temperatures, oxide layer thickness, hydrogen production rate, linear electrical rod power, steam and hydrogen mass flow rates.

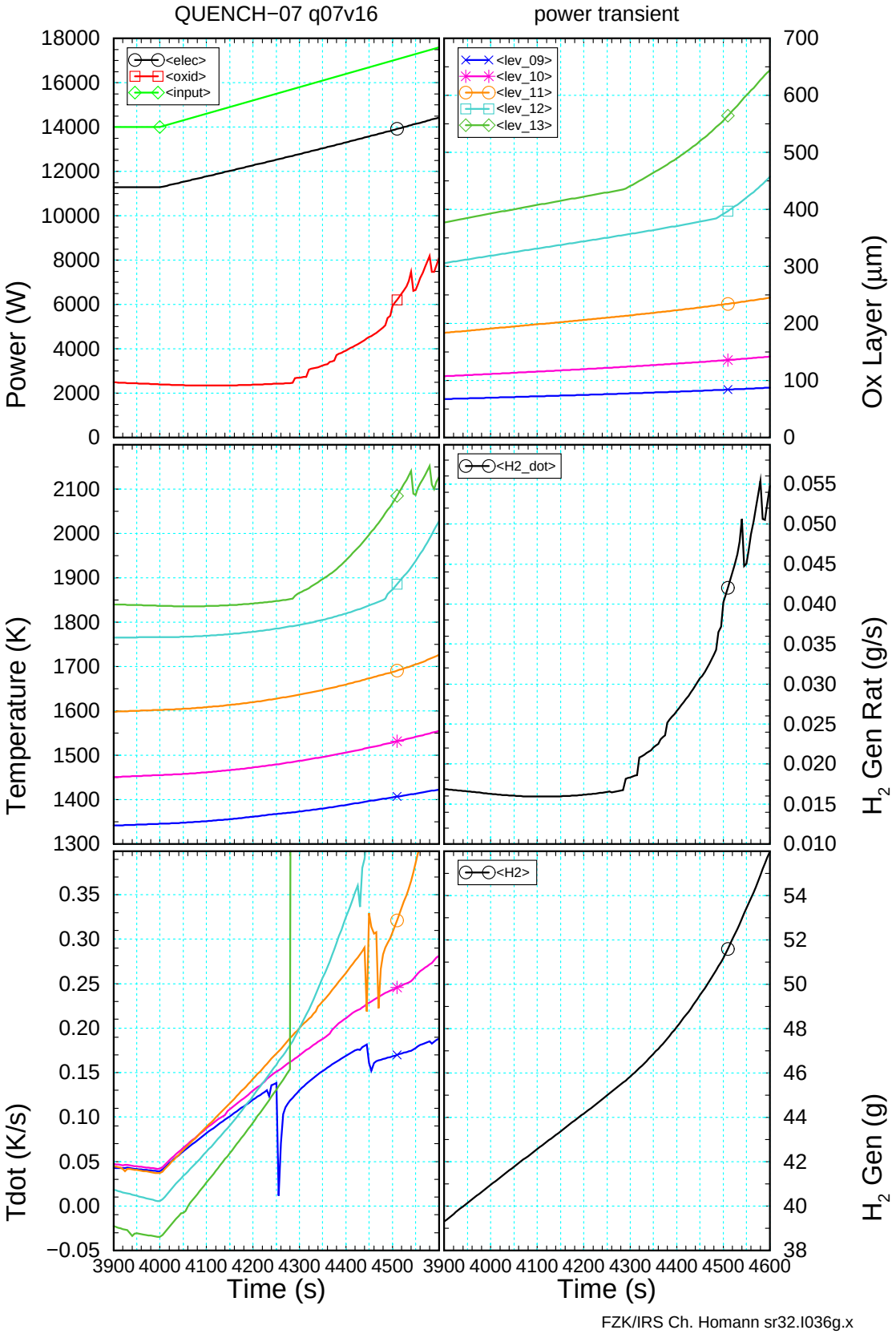

Fig. 14: FZK (FTP): selected variables for electrical power increase during test phase IV

The figure shows from top to bottom power, temperatures, and temperature increase at axial levels 9 to 13 (elevations 0.55 to 0.95 m, left), and oxide layer thickness at axial levels 9 to 13, total hydrogen production rate, and cumulated hydrogen mass (right) as a function of time.

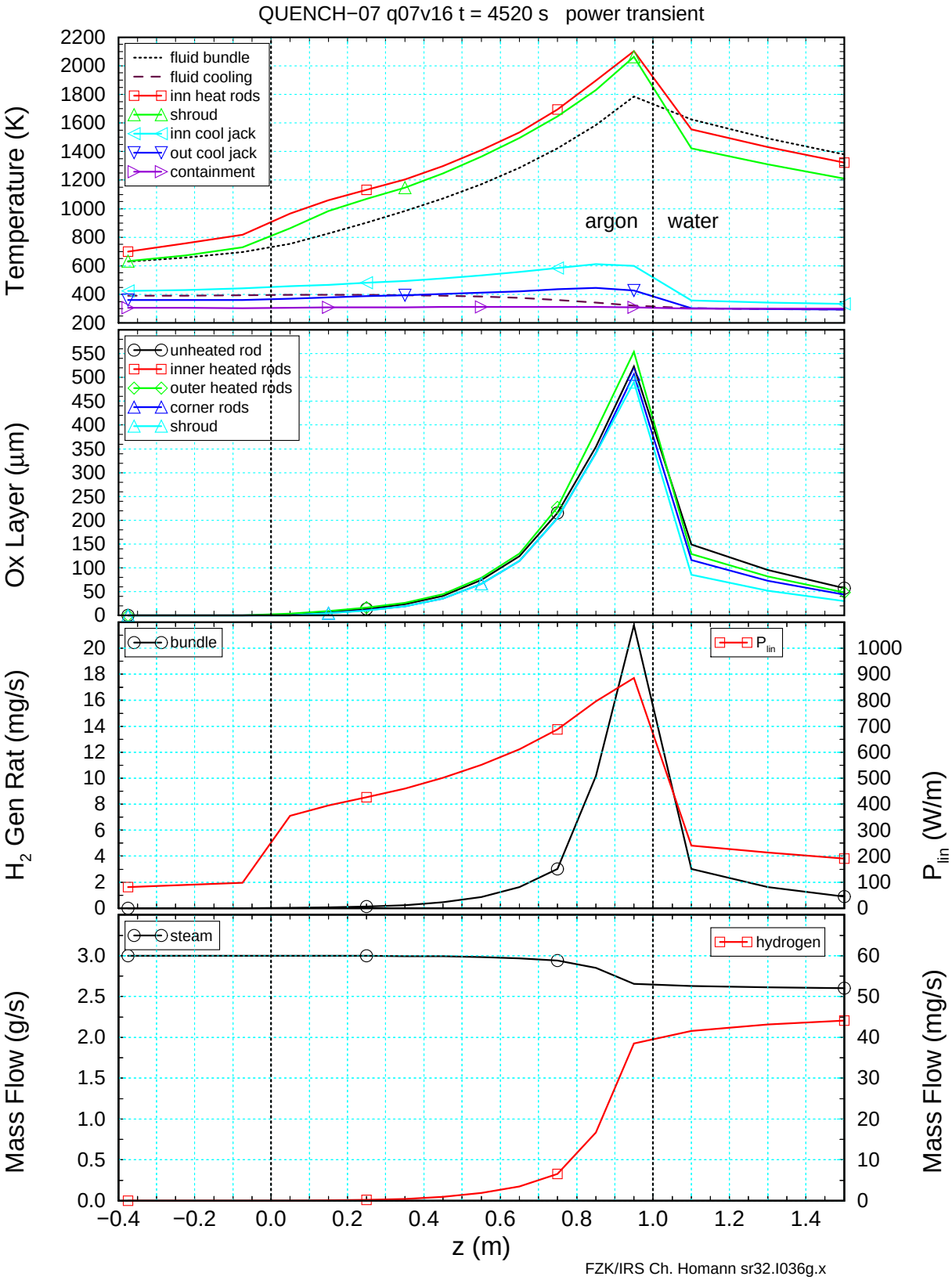

Fig. 15: FZK (FTP): axial profiles of selected variables for electrical power increase

The figure shows from top to bottom temperatures, oxide layer thickness, hydrogen production rate, linear electrical rod power, steam, and hydrogen mass flow rates during test phase IV.

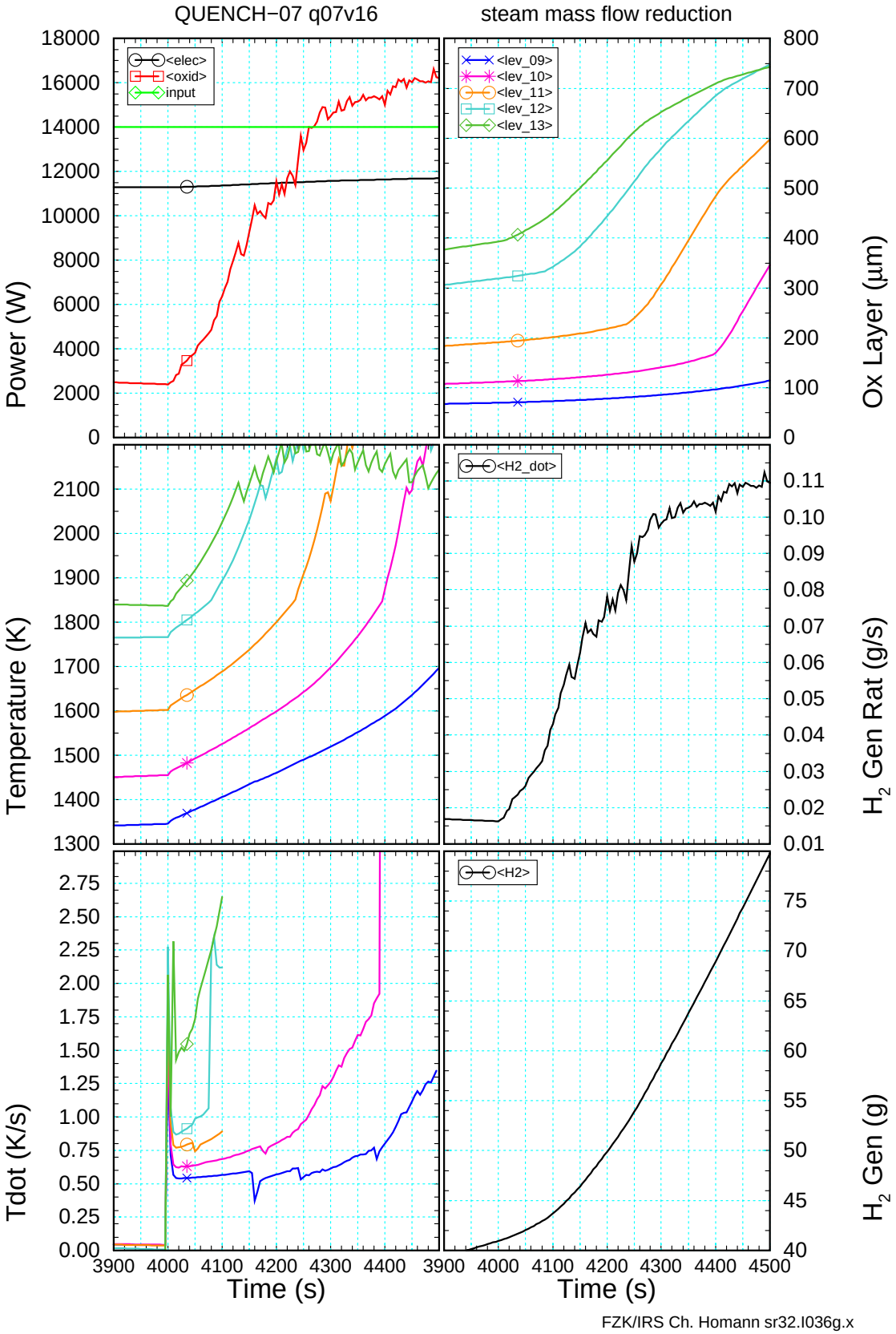

Fig. 16: FZK (FTP): selected variables for steam mass flow reduction

The figure shows from top to bottom power, temperatures, temperature increase at axial levels 9 to 13 (elevations 0.55 to 0.95 m) left), and oxide layer thickness at axial levels 9 to 13, total hydrogen production rate, and cumulated hydrogen mass for steam mass flow (right) during test phase IV as a function of time.

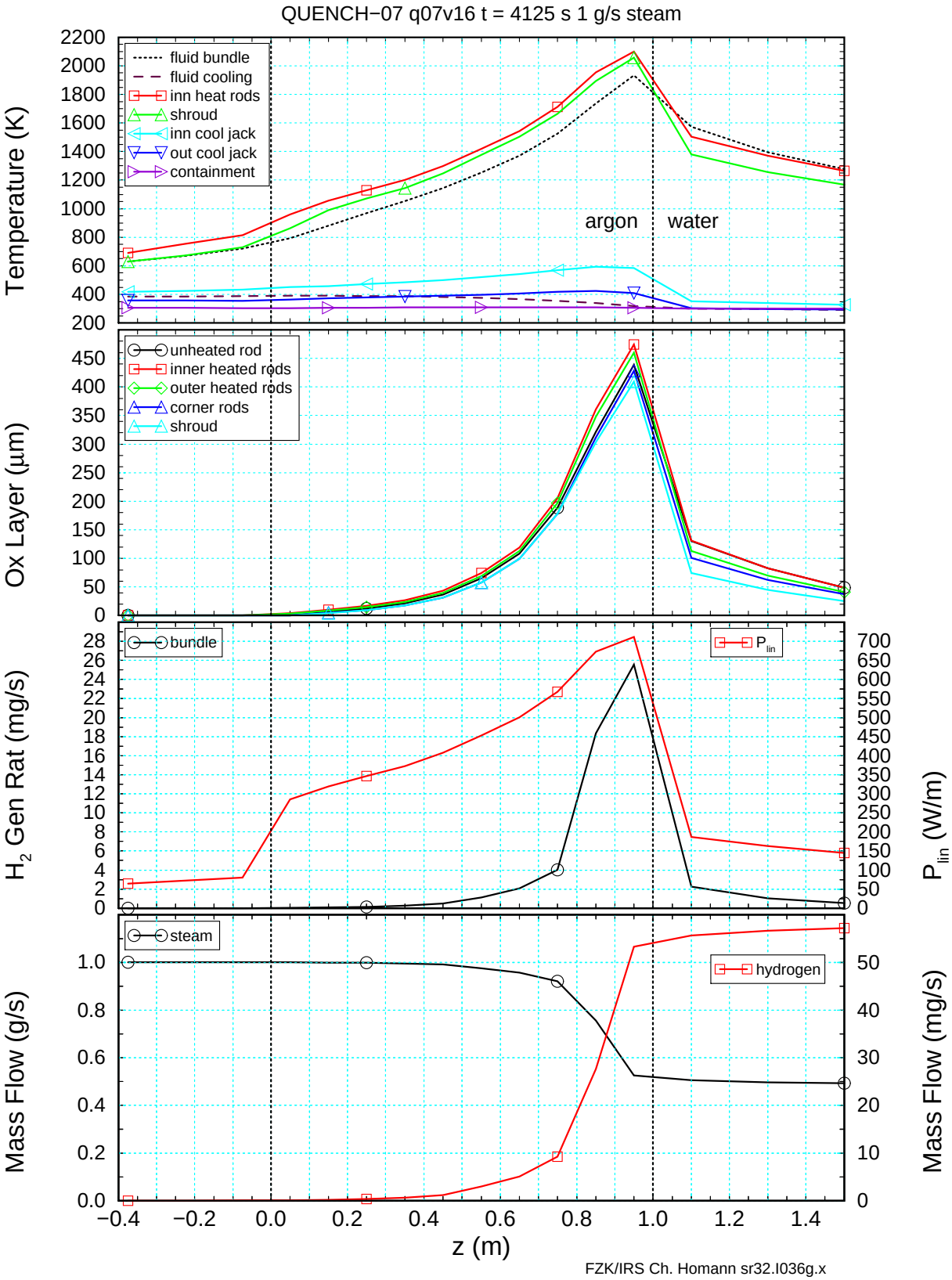

Fig. 17: FZK (FTP): axial profiles of selected variables for steam mass flow reduction

The figure shows from top to bottom temperatures, oxide layer thickness, hydrogen production rate, linear electrical rod power, steam, and hydrogen mass flow rates during test phase IV.

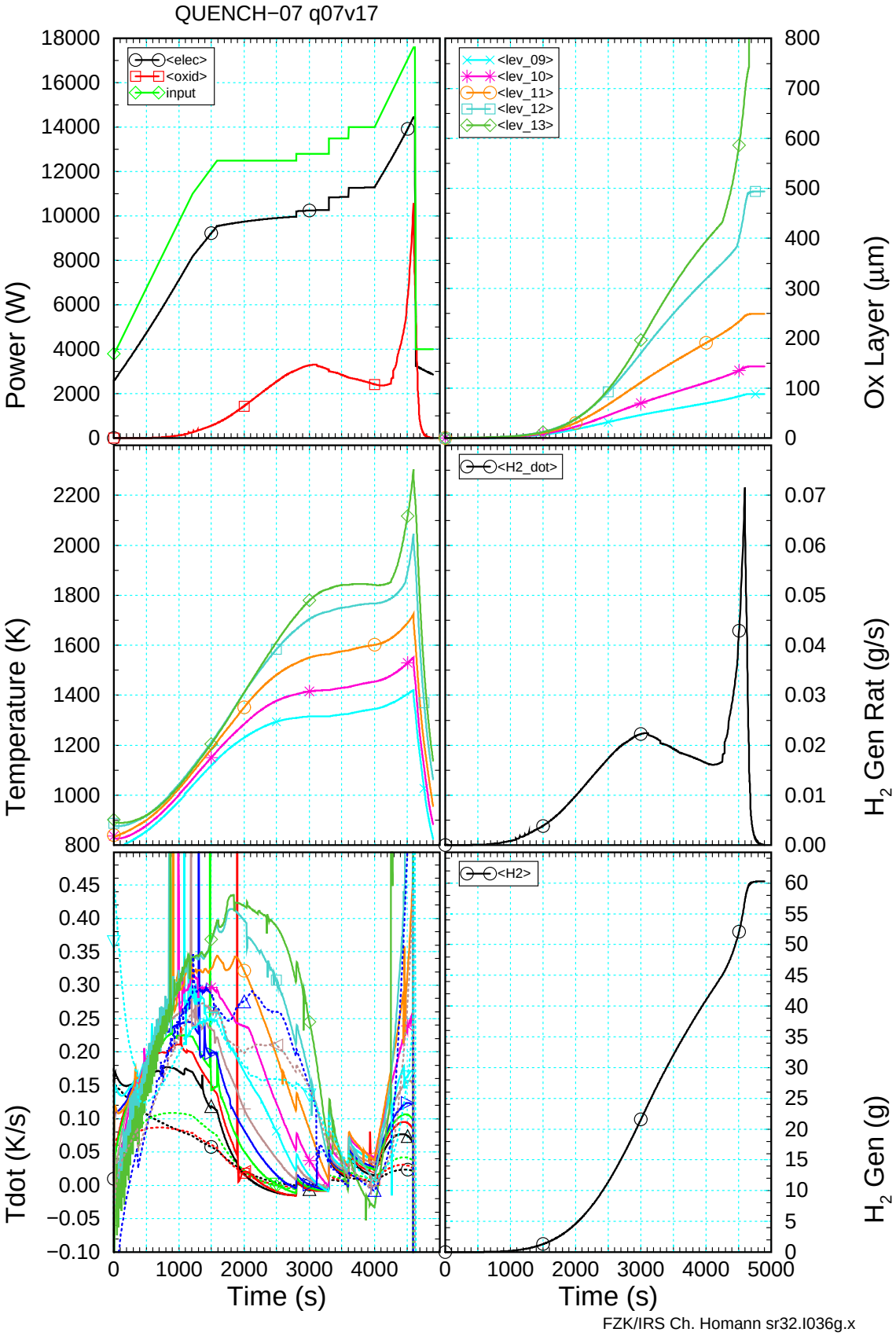

Fig. 18: FZK (FTP): selected variables for the whole test

The figure shows power, temperatures, temperature increase at axial levels 9 to 13 (elevations 0.55 to 0.95 m) left), and oxide layer thickness at axial levels 9 to 13, total hydrogen production rate, and cumulated hydrogen mass (right) as a function of time.

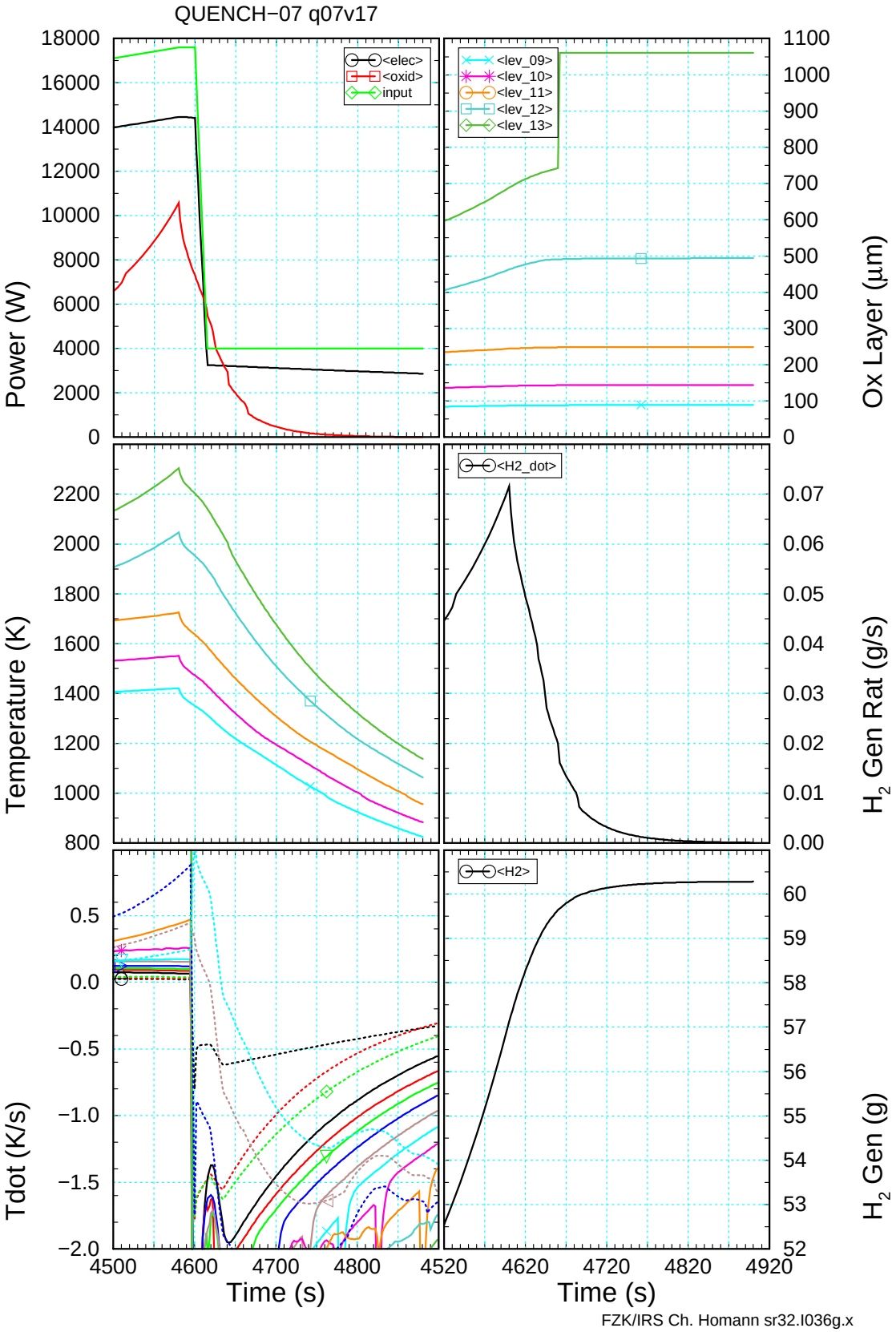

Fig. 19: FZK (FTP): selected variables during cool-down (test phase V)

The figure shows power, temperatures, temperature increase at axial levels 9 to 13 (elevations 0.55 to 0.95 m, left), and oxide layer thickness at axial levels 9 to 13, total hydrogen production rate, and cumulated hydrogen mass (right) as a function of time.

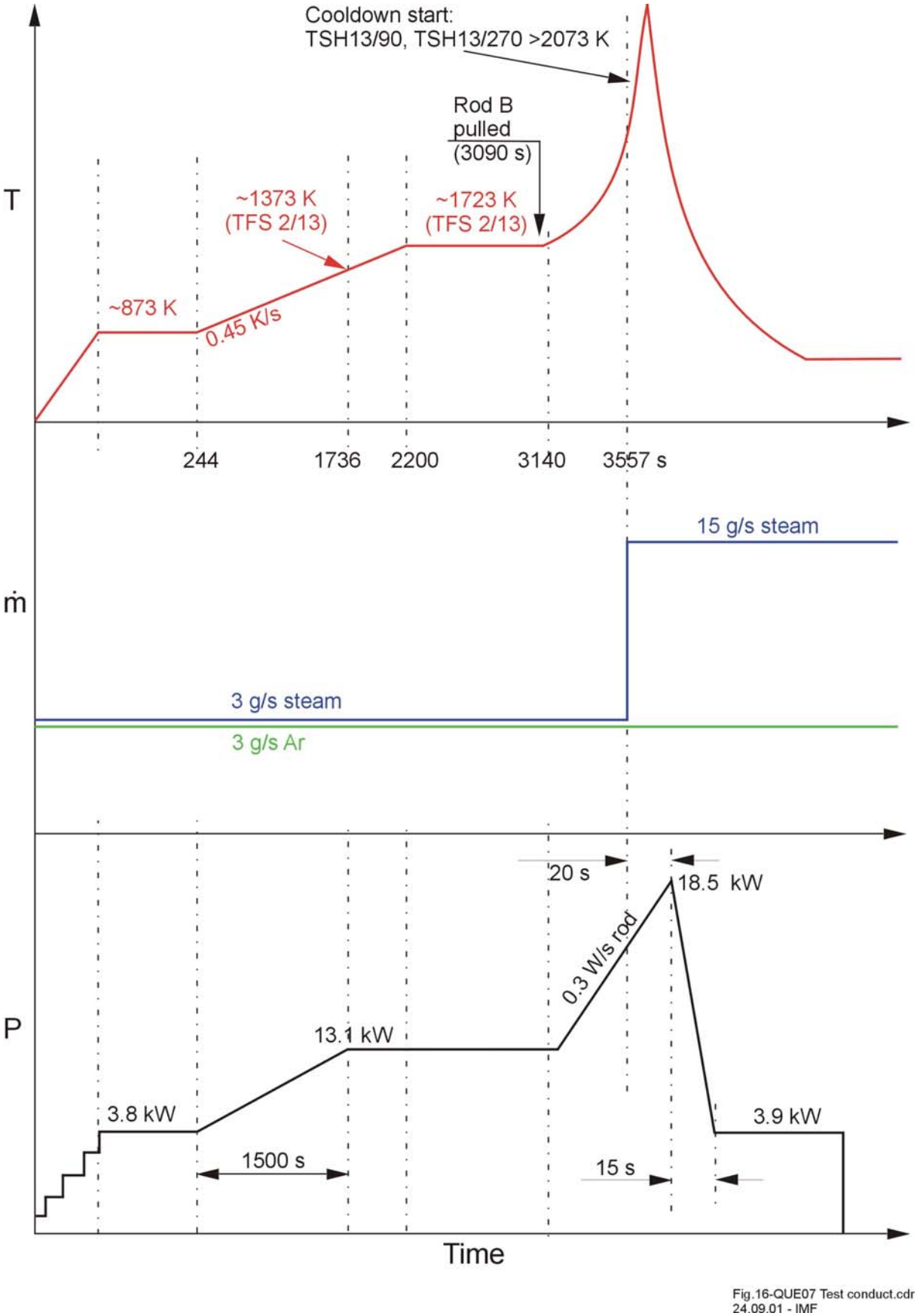

Fig. 20: Conduct of test QUENCH-07

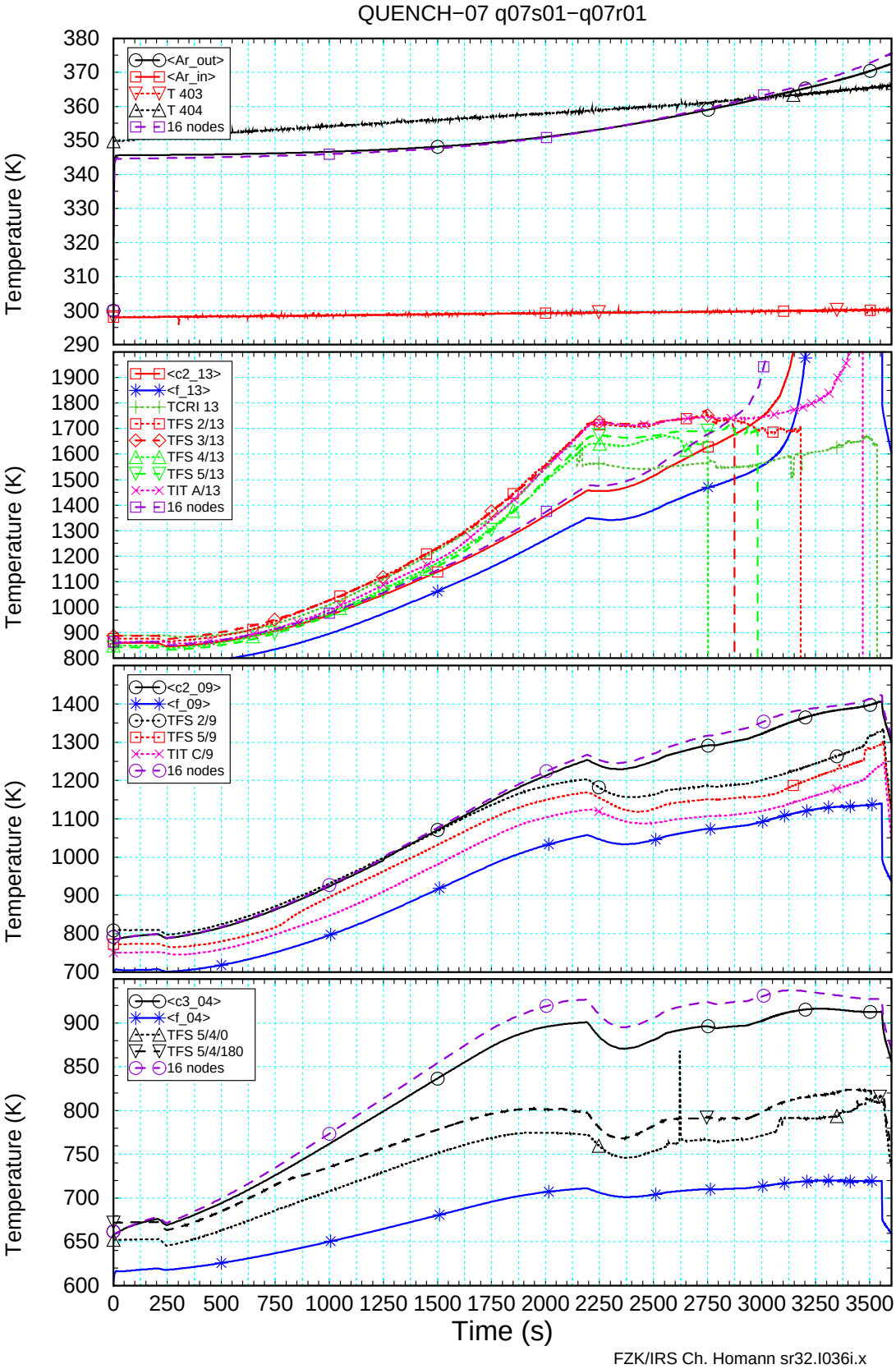

Fig. 21: FZK post-test calculation: comparison of measured and calculated temperatures

The figure shows from top to bottom temperatures in the argon cooling and in the bundle at axial levels 13, 9, and 4 (elevations 0.95, 0.55, 0.05 m), respectively, as a function of time. “<c2…>”, “<c3…>” and “<f…>” refer to inner, outer clad, and fluid temperatures, calculated with the 32f model, “16 nodes” refers to the 16f model.

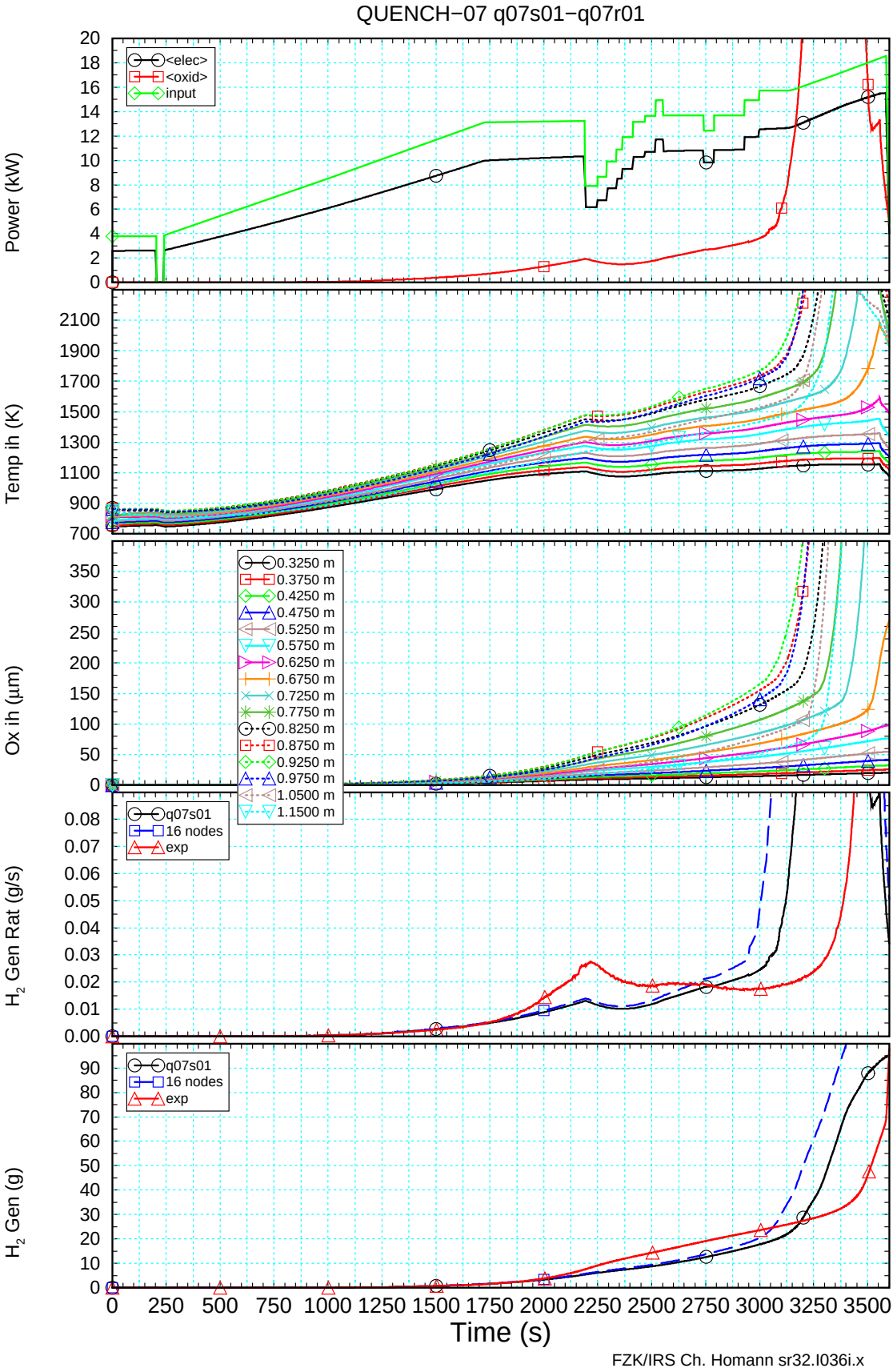

Fig. 22: FZK post test calculation: selected variables as a function of time

The figure shows from top to bottom power, calculated temperatures and oxide layer thickness, measured and calculated hydrogen production rate and cumulated hydrogen mass.

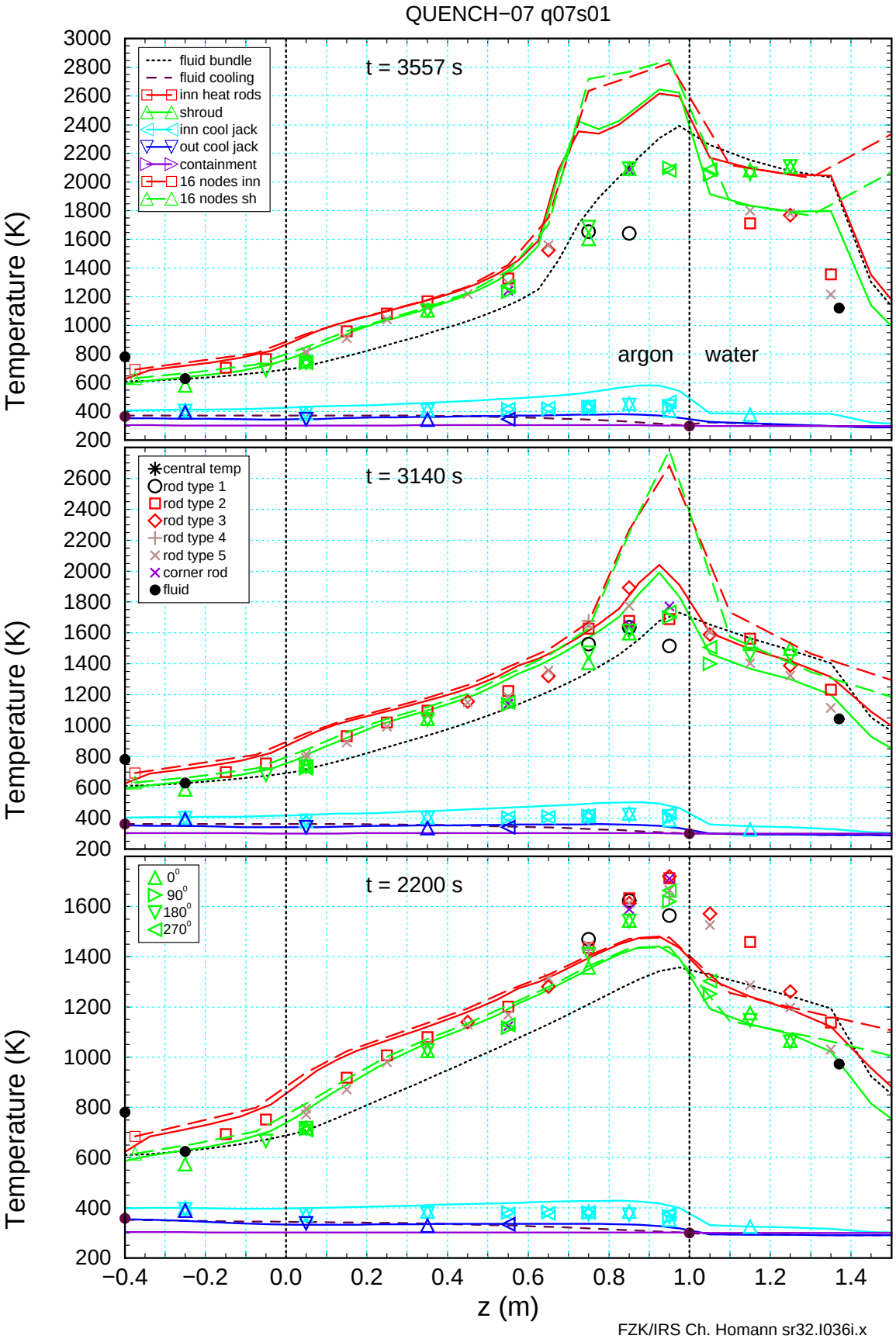

Fig. 23: FZK post test calculation: axial profiles of temperatures, part 1

The figure shows from top to bottom measured and calculated axial profiles of temperatures, at the beginning of phase V, IV, and III, respectively.

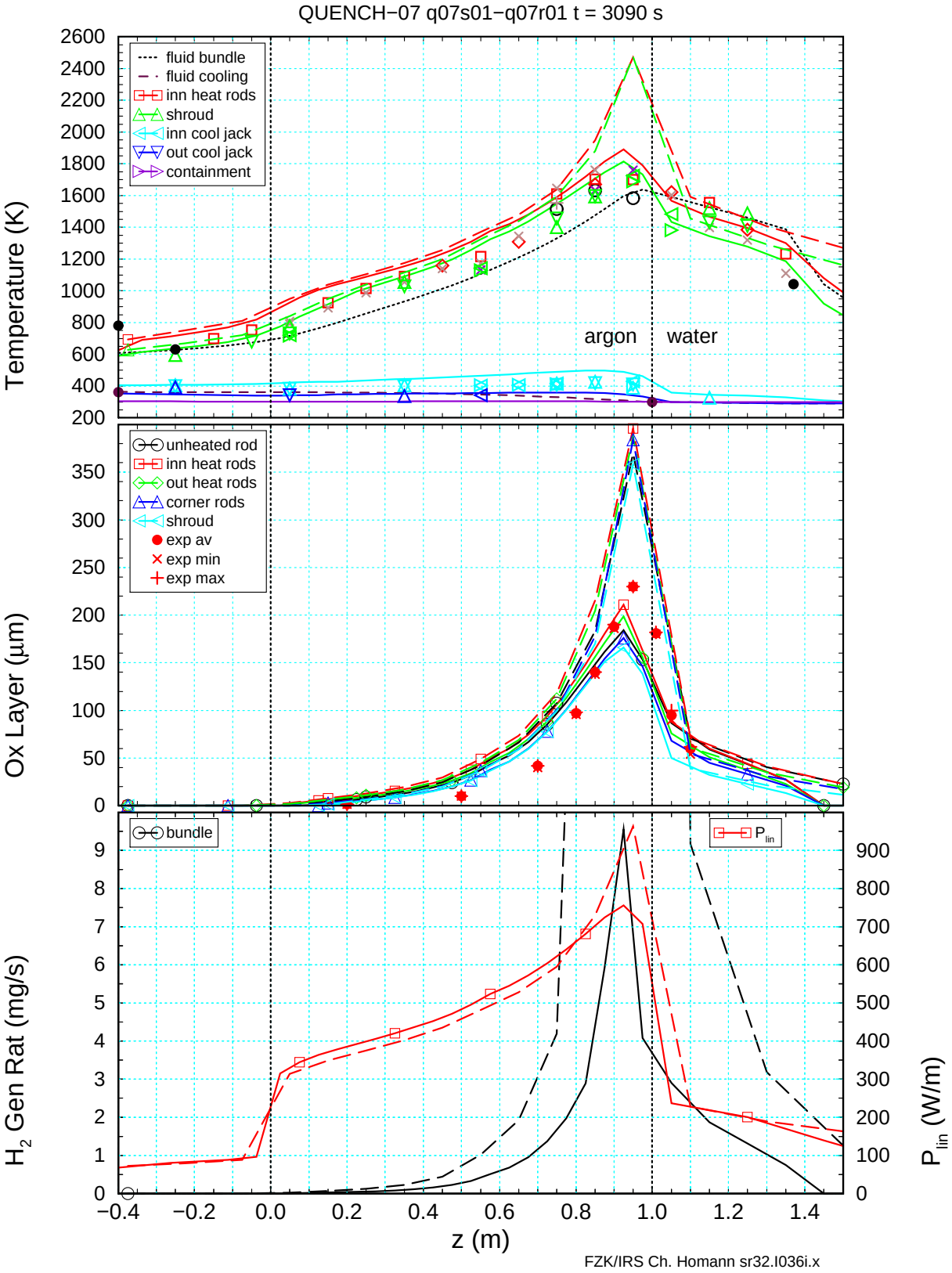

Fig. 24: FZK post test calculation: axial profiles of selected variables (part 2)

The figure shows from top to bottom measured and calculated axial profiles of temperatures, oxide layer thickness, hydrogen production rate, and linear electrical rod power at the time of withdrawal of a corner rod.

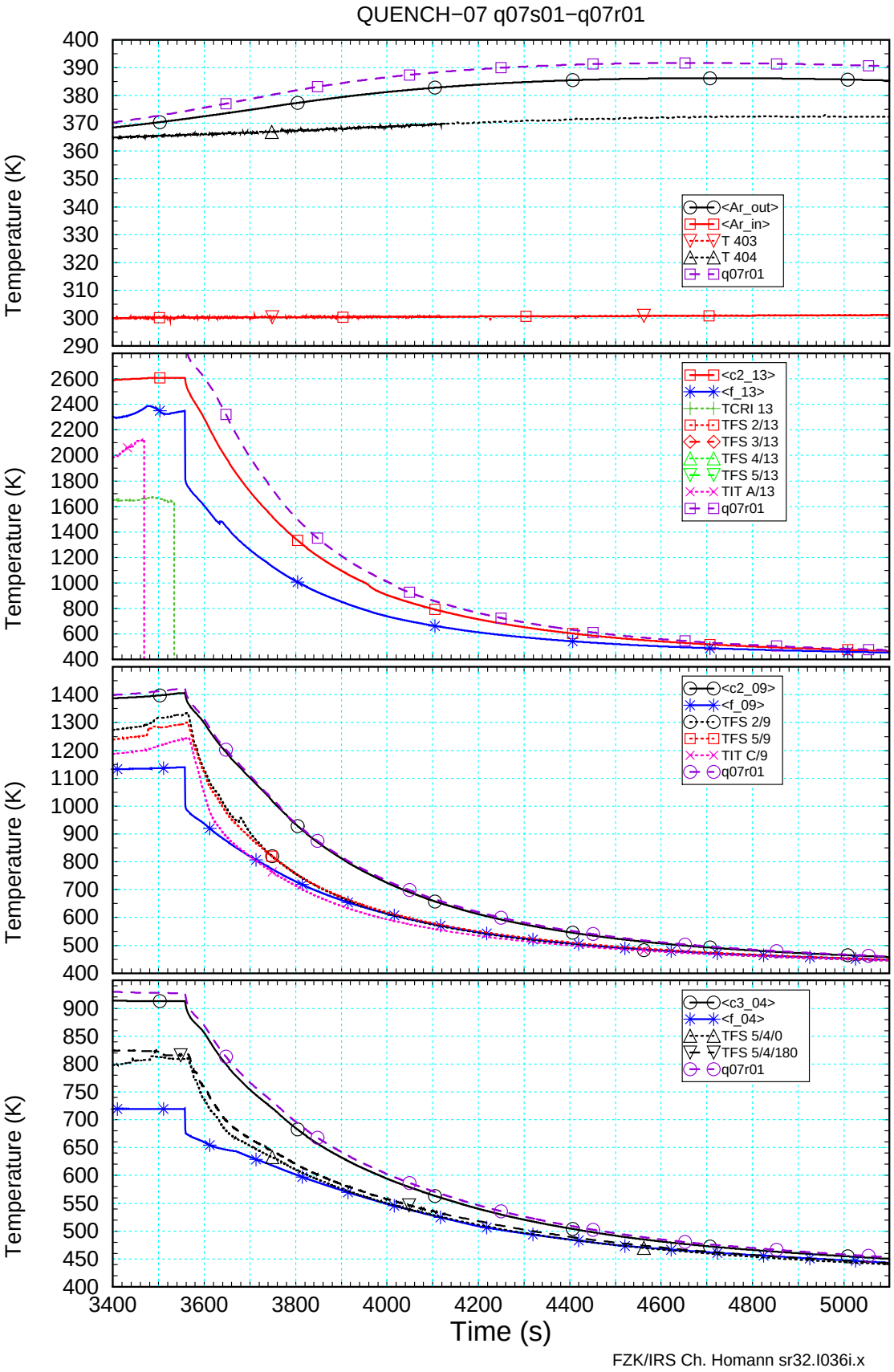

Fig. 25: FZK post-test calculation: temperatures during cool-down

The figure shows from top to bottom measured and calculated temperatures in the argon cooling and in the bundle at axial levels 4, 9, and 13 (elevations 0.95, 0.55, 0.05 m), respectively, during cool-down.

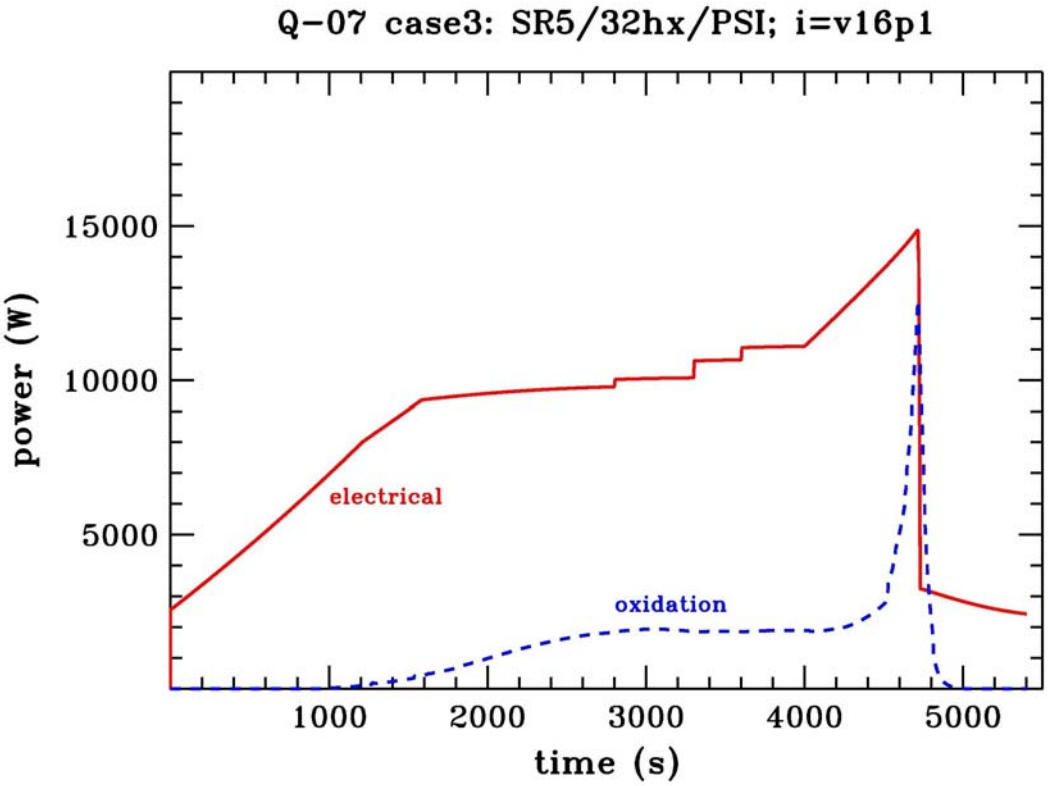

Fig. 26: PSI: power release in the bundle (baseline case)

The figure shows electrical and chemical power released in the bundle as a function of time.

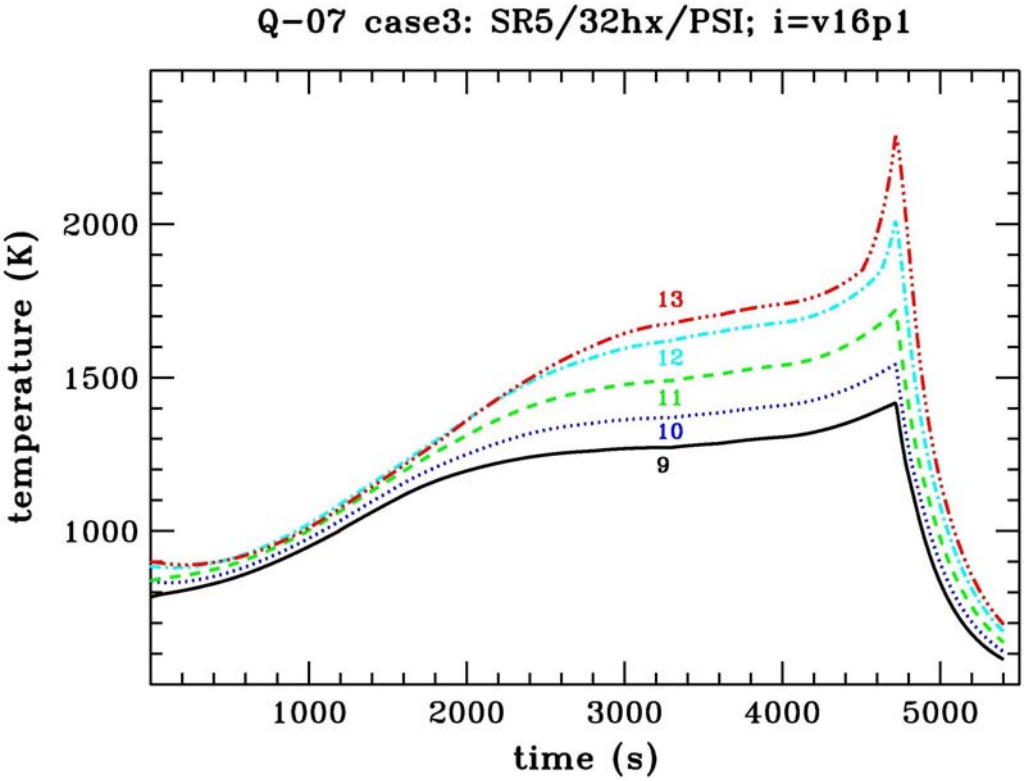

Fig. 27: PSI: cladding temperatures (baseline case)

The figure shows temperatures of the inner heated rods at various axial locations as a function of time.

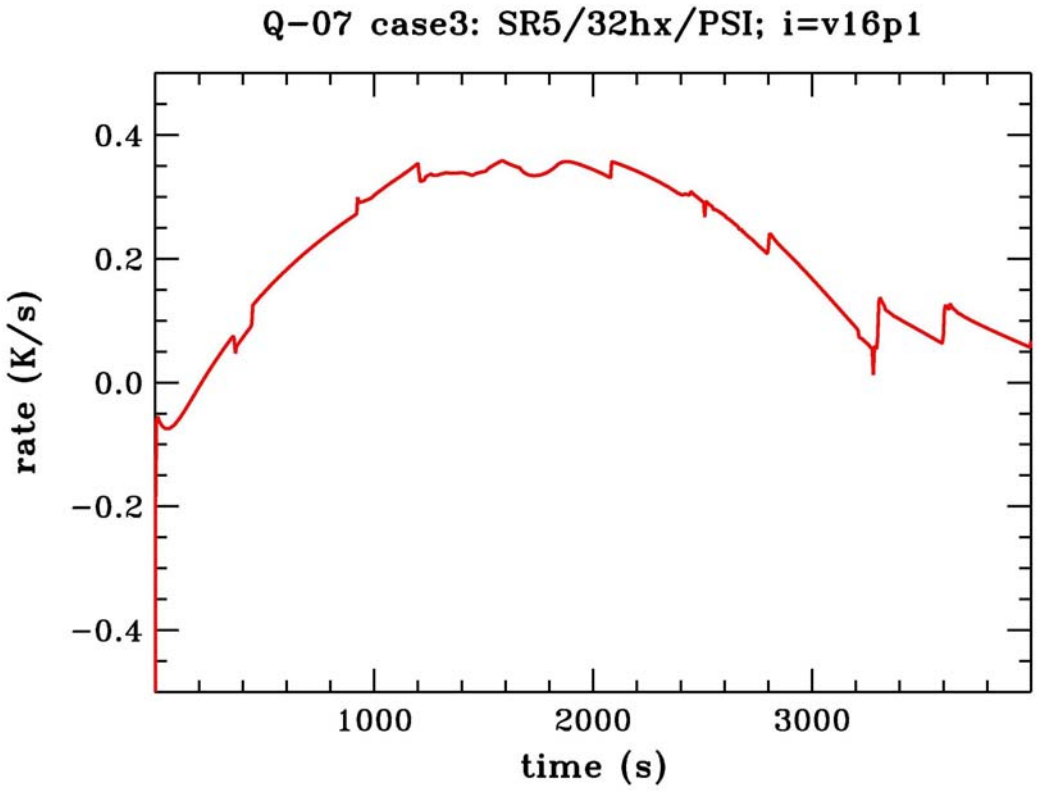

Fig. 28: PSI: cladding temperature rise during phase III (baseline case)

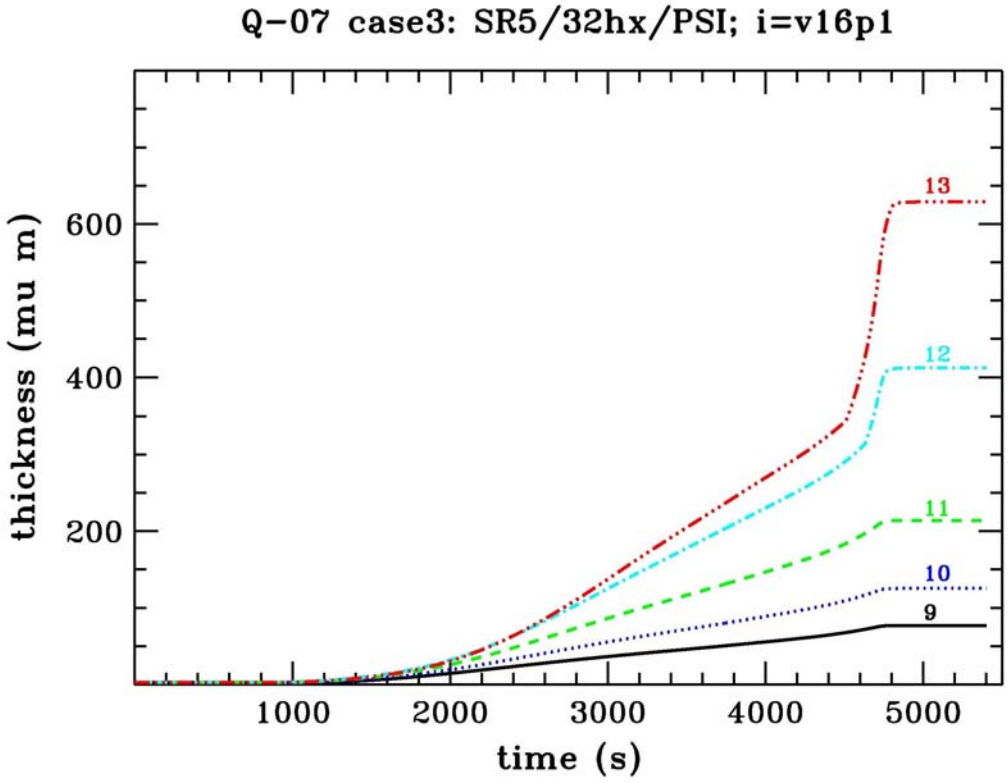

Fig. 29: PSI: oxide layer thickness (baseline case)

The figure shows oxide layer thickness in the inner heated ring at various axial locations as a function of time.

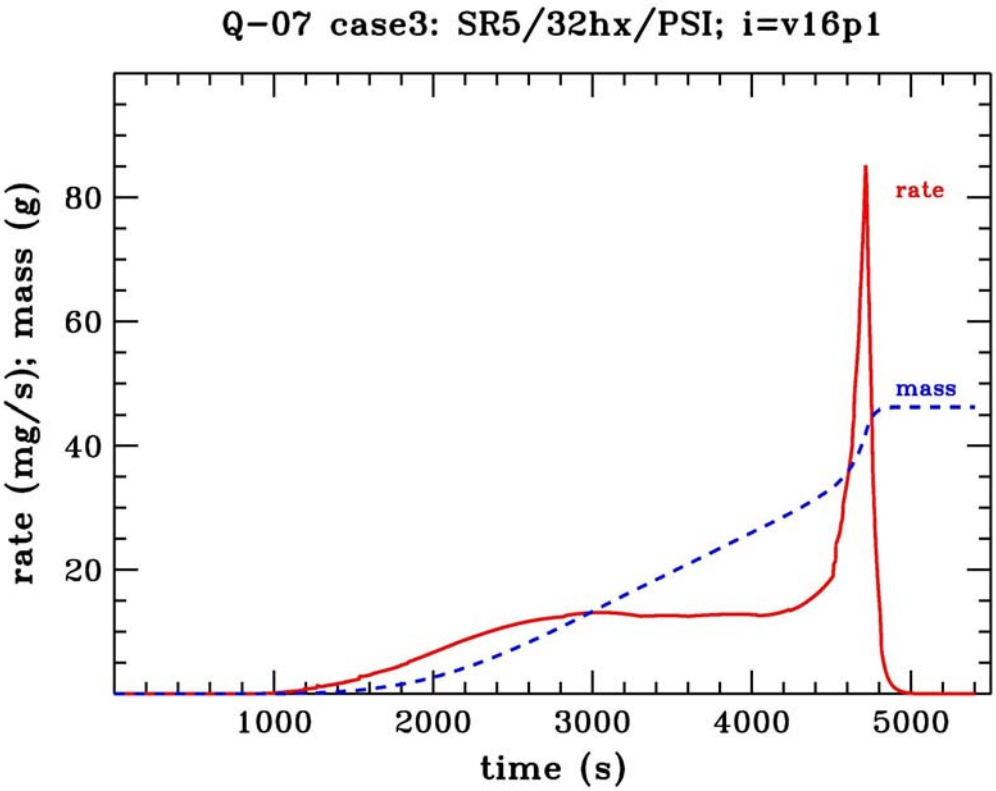

Fig. 30: PSI: hydrogen production and cumulated hydrogen mass (baseline case)

The figure shows hydrogen production rate (red) and total mass (blue) as a function of time.

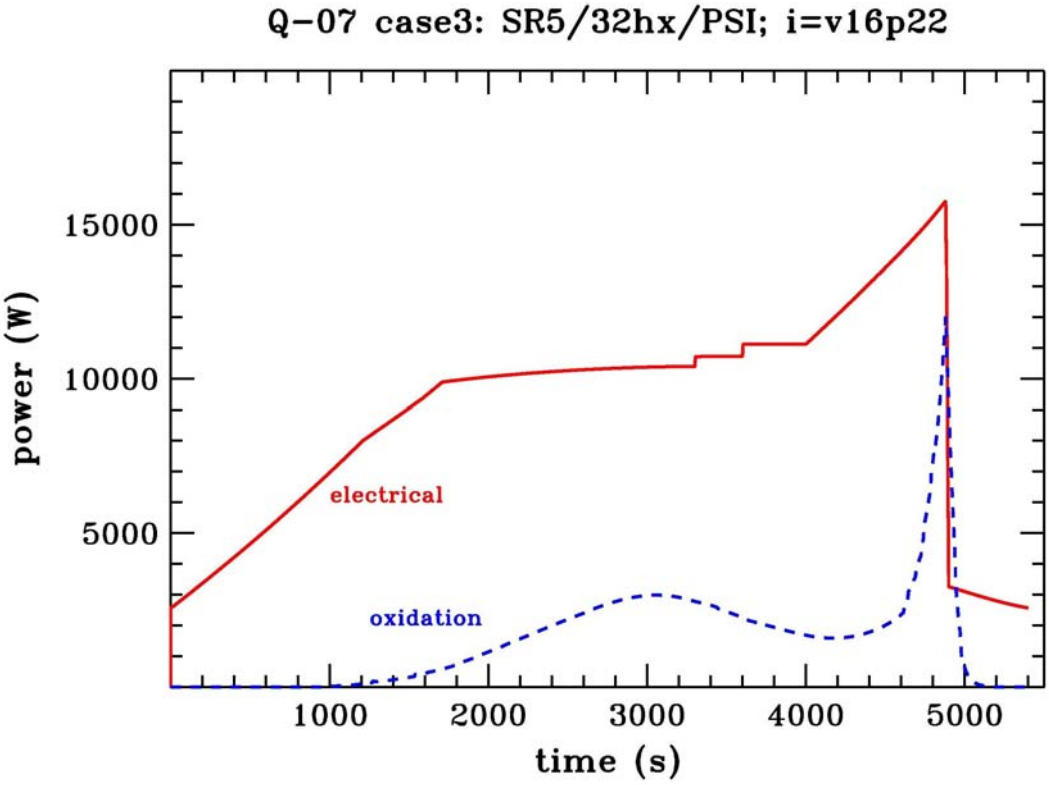

Fig. 31: PSI: power release in the bundle (modified case)

The figure shows electrical and chemical power released in the bundle as a function of time.

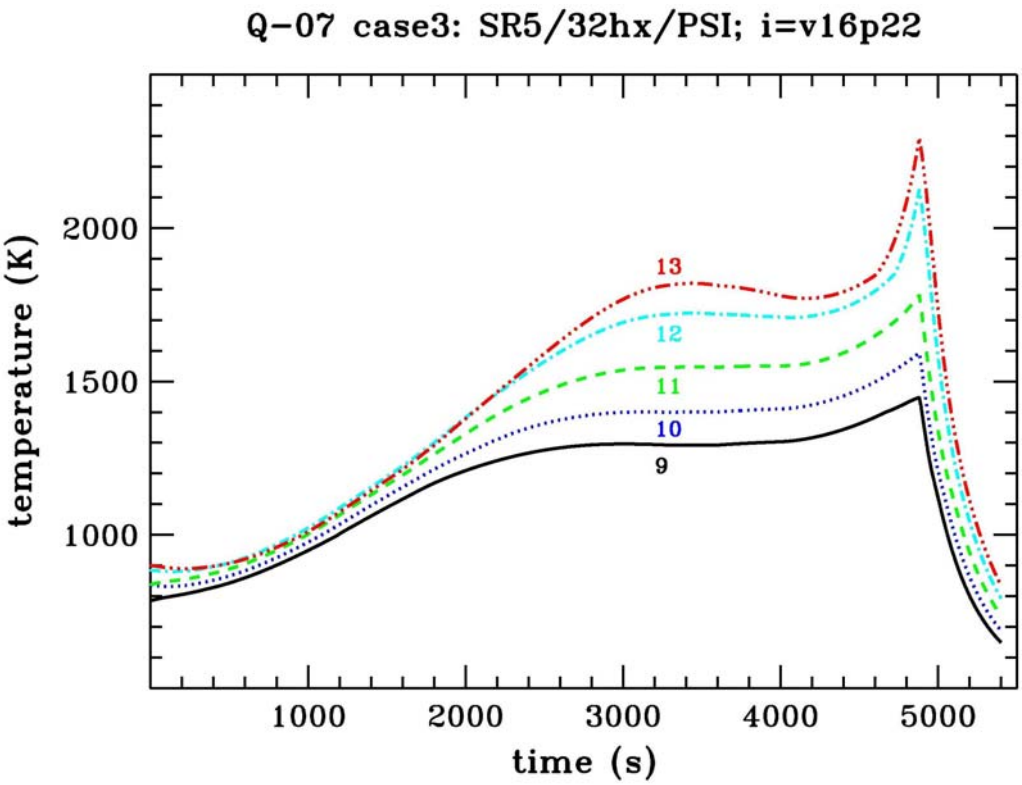

Fig. 32: PSI: cladding temperatures (modified case)

The figure shows temperatures of the inner heated rods at various axial locations as a function of time.

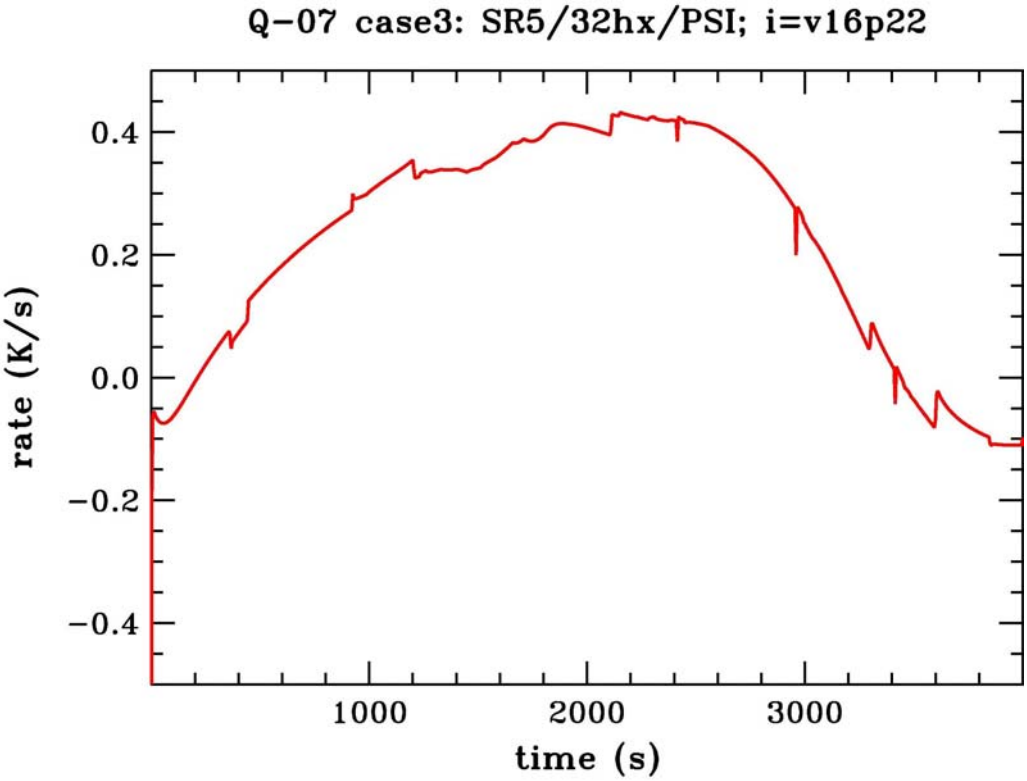

Fig. 33: PSI: cladding temperature rise during phase III (modified case)

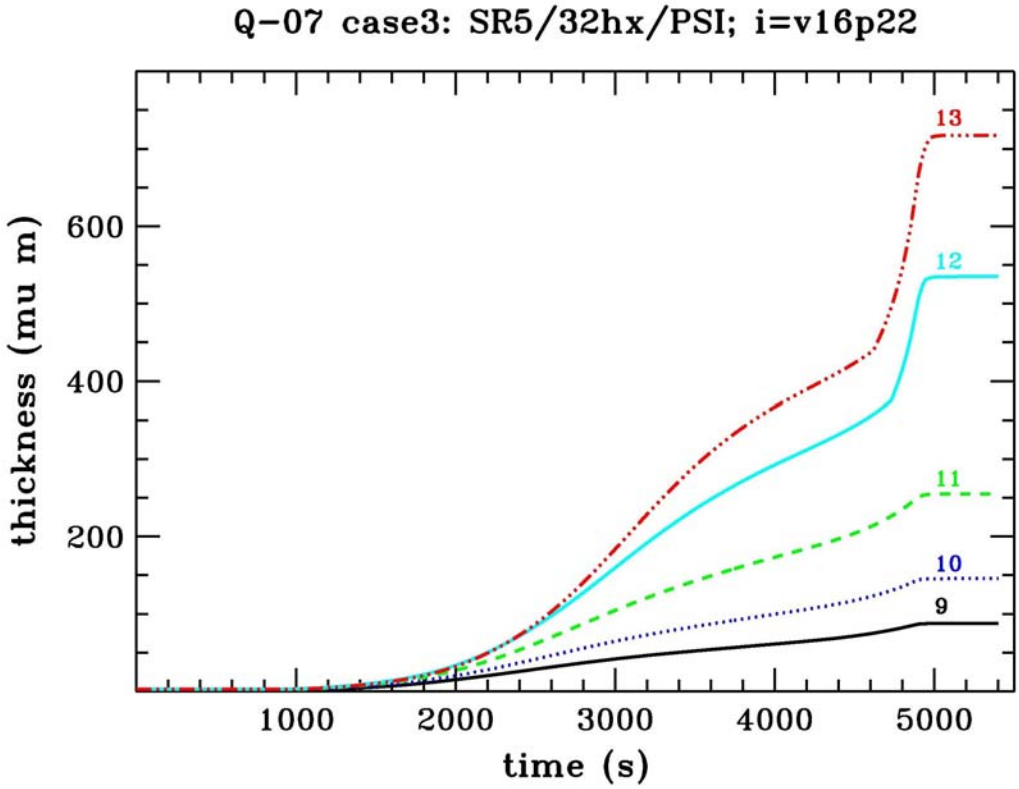

Fig. 34: PSI: oxide layer thickness (modified case)

The figure shows oxide layer thickness in the inner heated ring at various axial locations as a function of time.

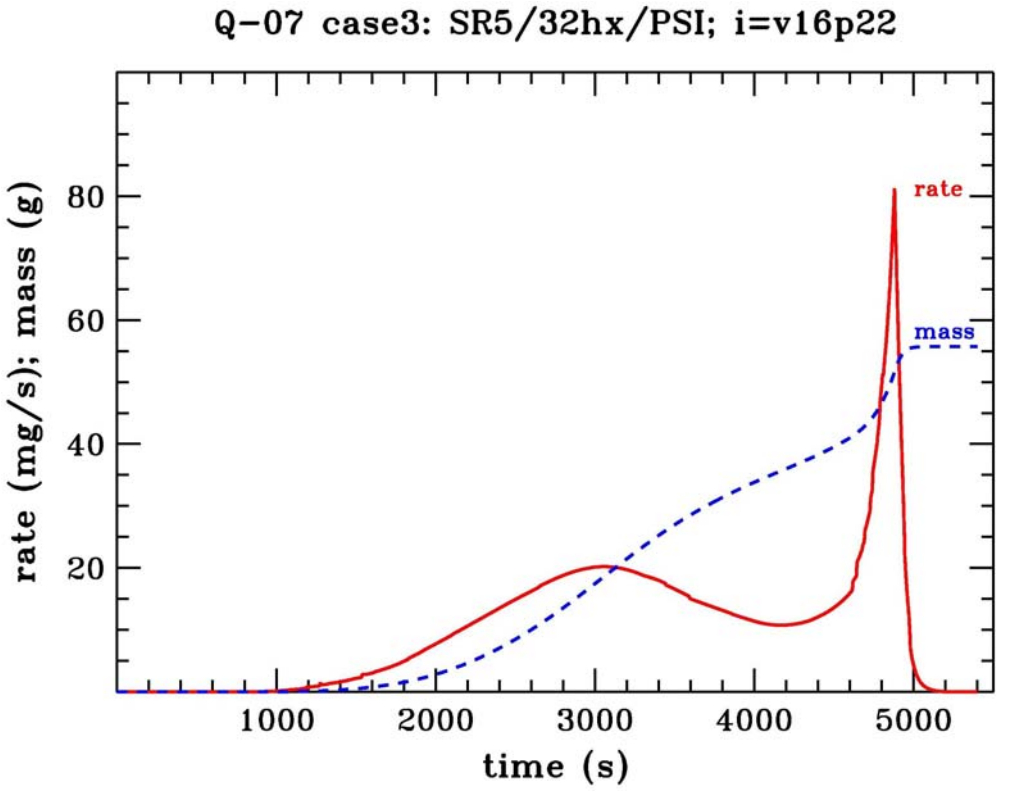

Fig. 35: PSI: hydrogen production and cumulated hydrogen mass (modified case)

The figure shows hydrogen production rate (red) and total mass (blue) as a function of time.

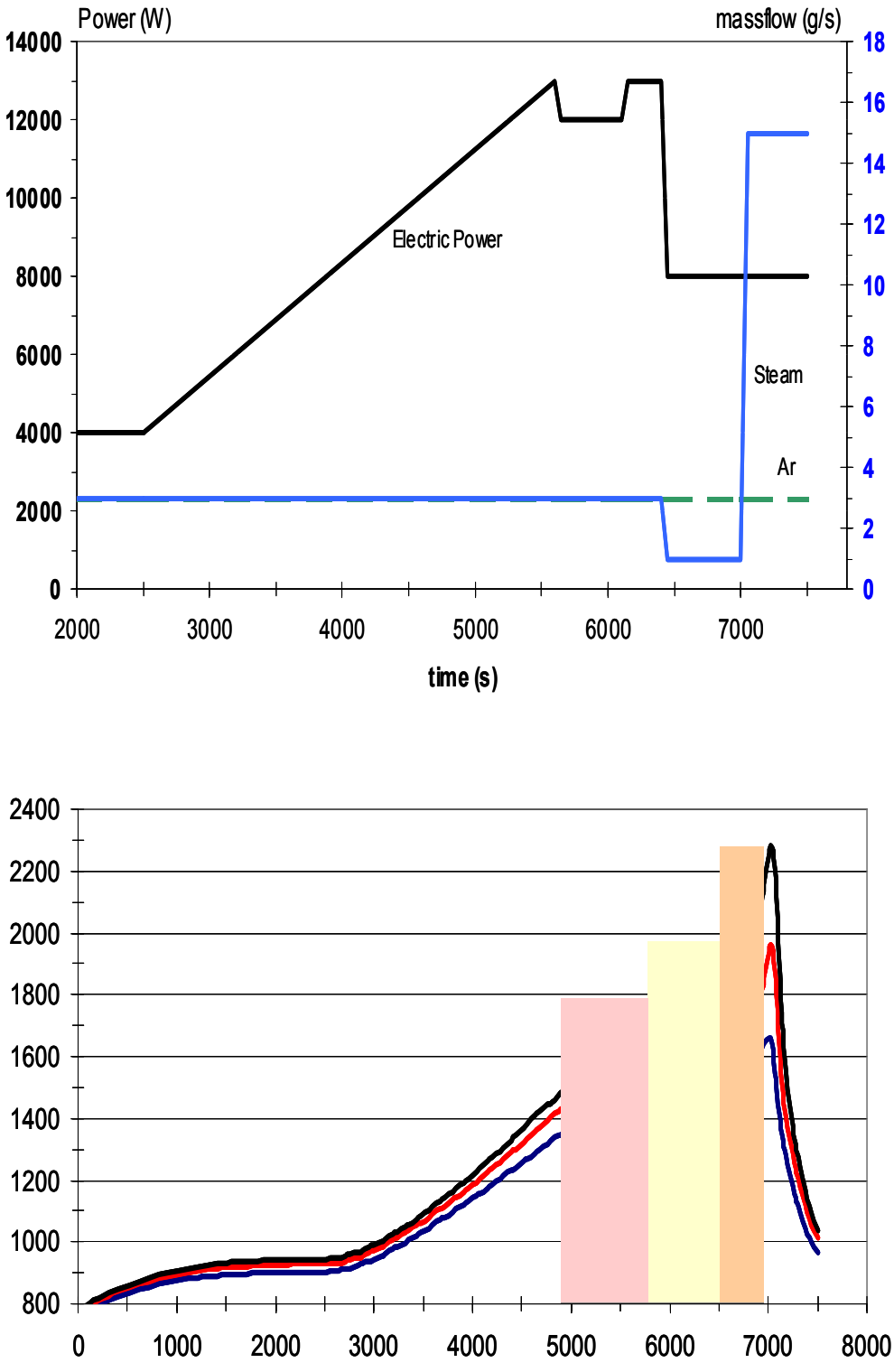

Fig. 36: UPM: electrical power, gas mass flow, and temperature history (case 0)

The figure shows electrical power in W (left) and gas mass flow history in g/s (right) in the top and time evolution of temperatures in K at different levels in the bottom.

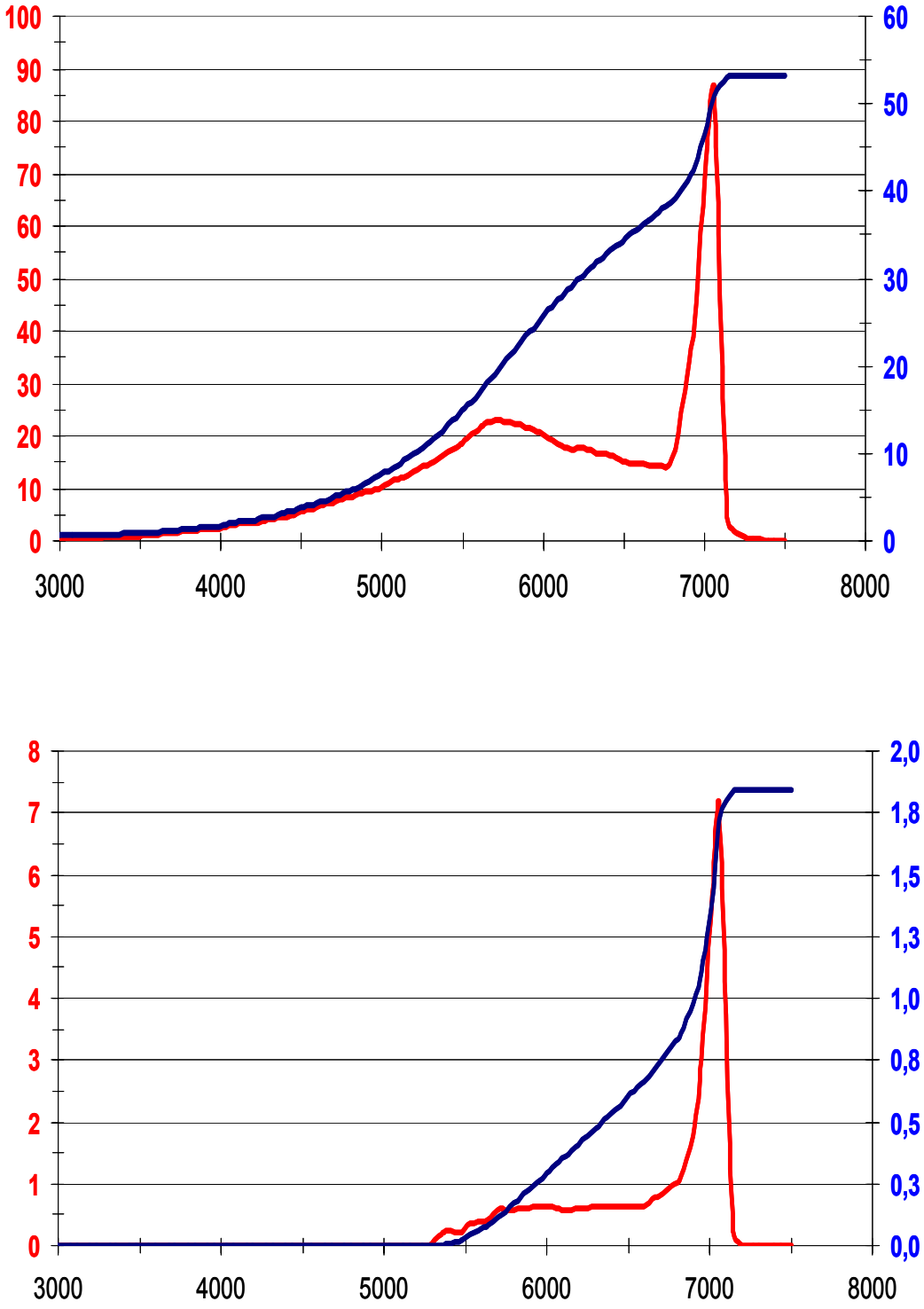

Fig. 37: UPM: total hydrogen production and H_2 generation due to B_4C oxidation (case 0)

The figure shows the total hydrogen production (top) and H_2 generation due to B_4C oxidation (bottom). Red lines refer to the rate in mg/s and blue lines to total accumulated mass in g.

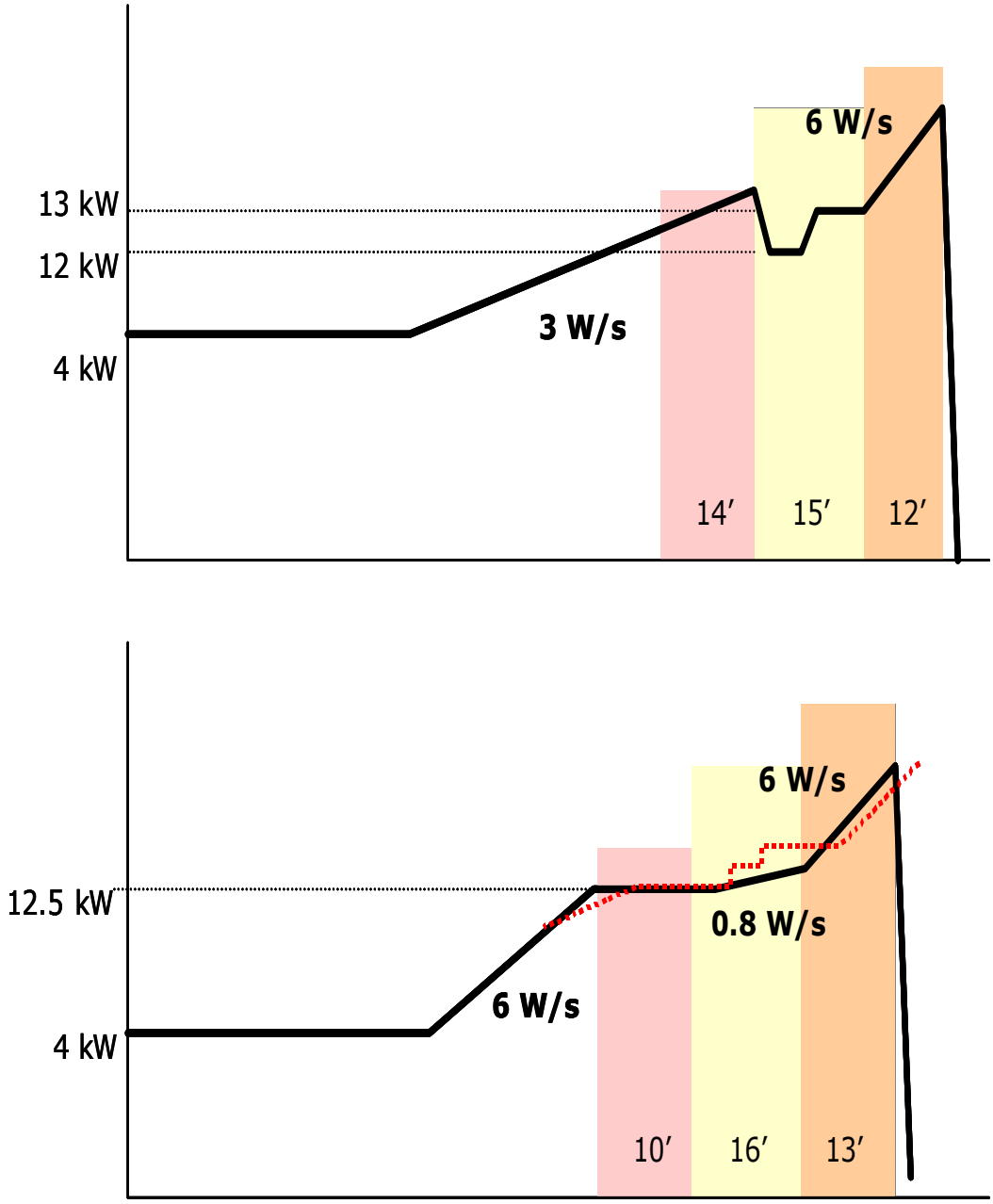

Fig. 38: UPM: electric power profile and duration of main phases (cases 1 and 2)

The figure shows results for case 1 (top) and case 2 (bottom).

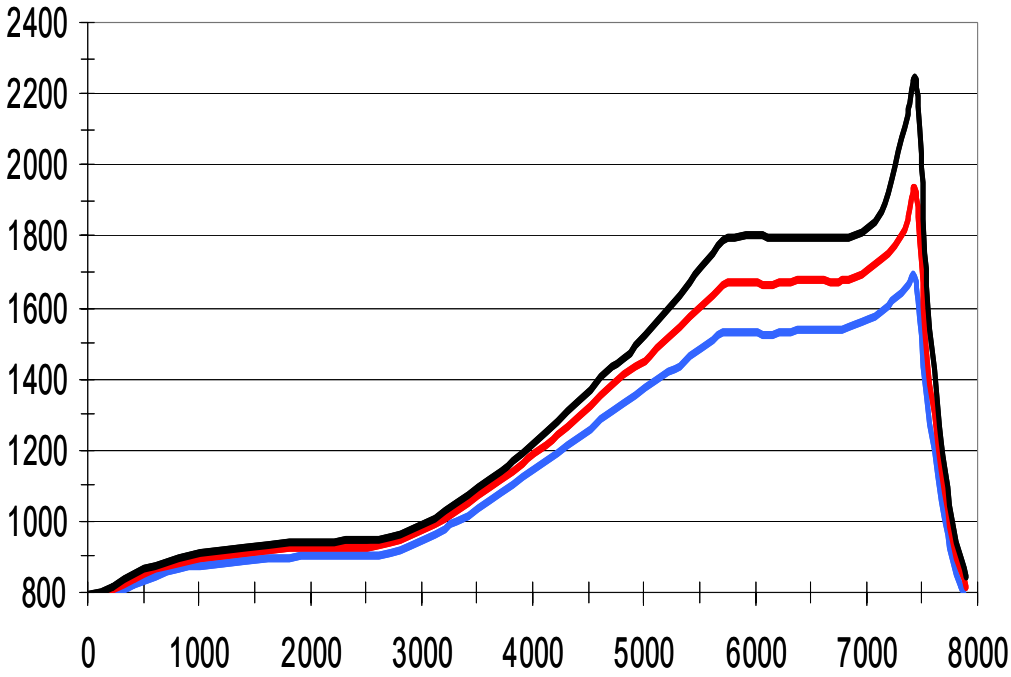

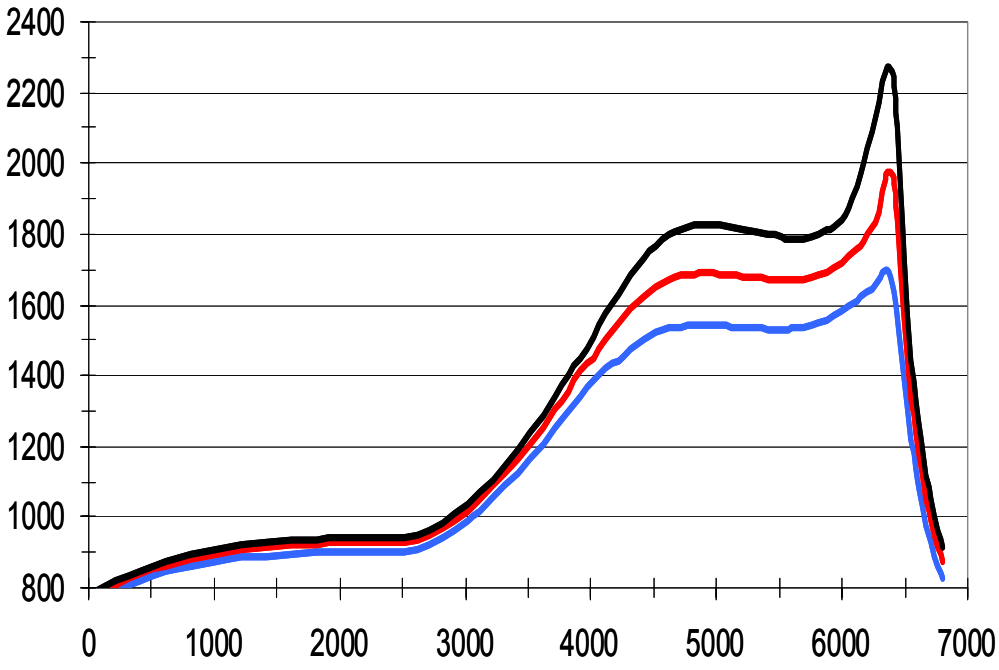

Fig. 39: UPM: temperatures for cases 1 and 2

The figure shows time evolution of temperatures in K at different levels for case 1 (top) and case 2 (bottom).

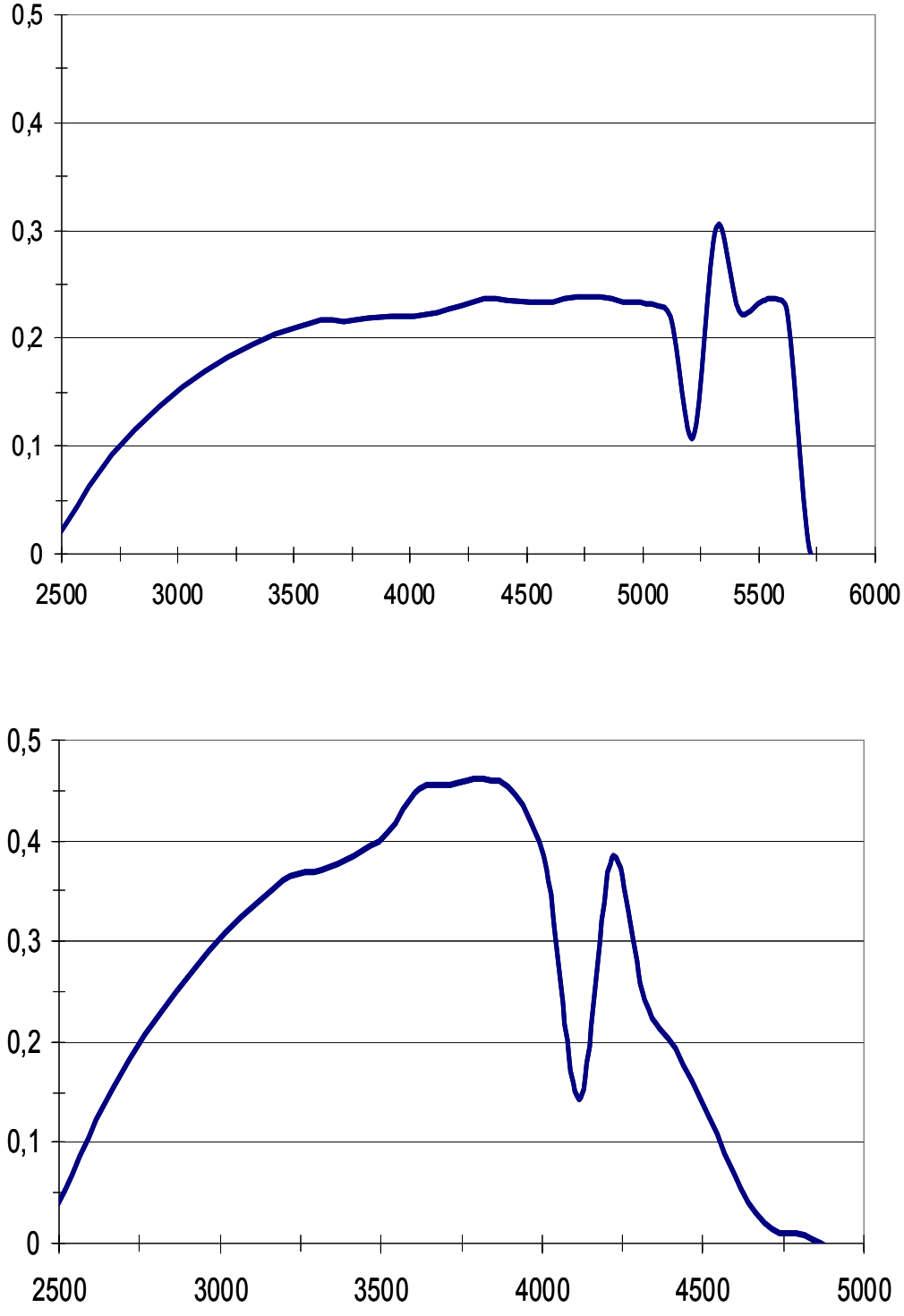

Fig. 40: UPM: bundle heating rate for cases 1 and 2

The figure shows results for case 1 (top) and case 2 (bottom).

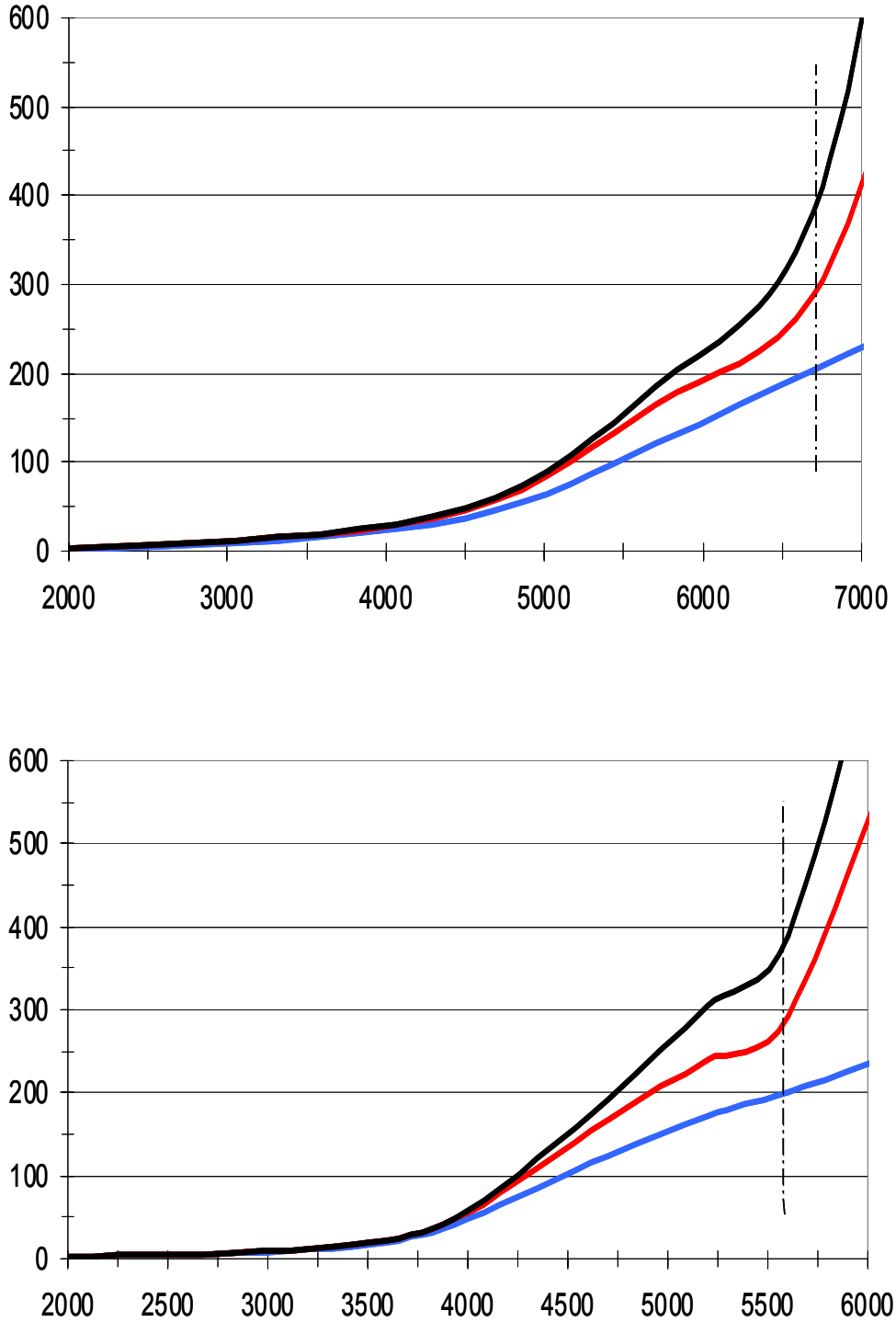

Fig. 41: UPM: oxide layer thickness for cases 1 and 2

The figure shows the thickness of cladding oxide layer in µm at different levels for case 1 (top) and case 2 (bottom).

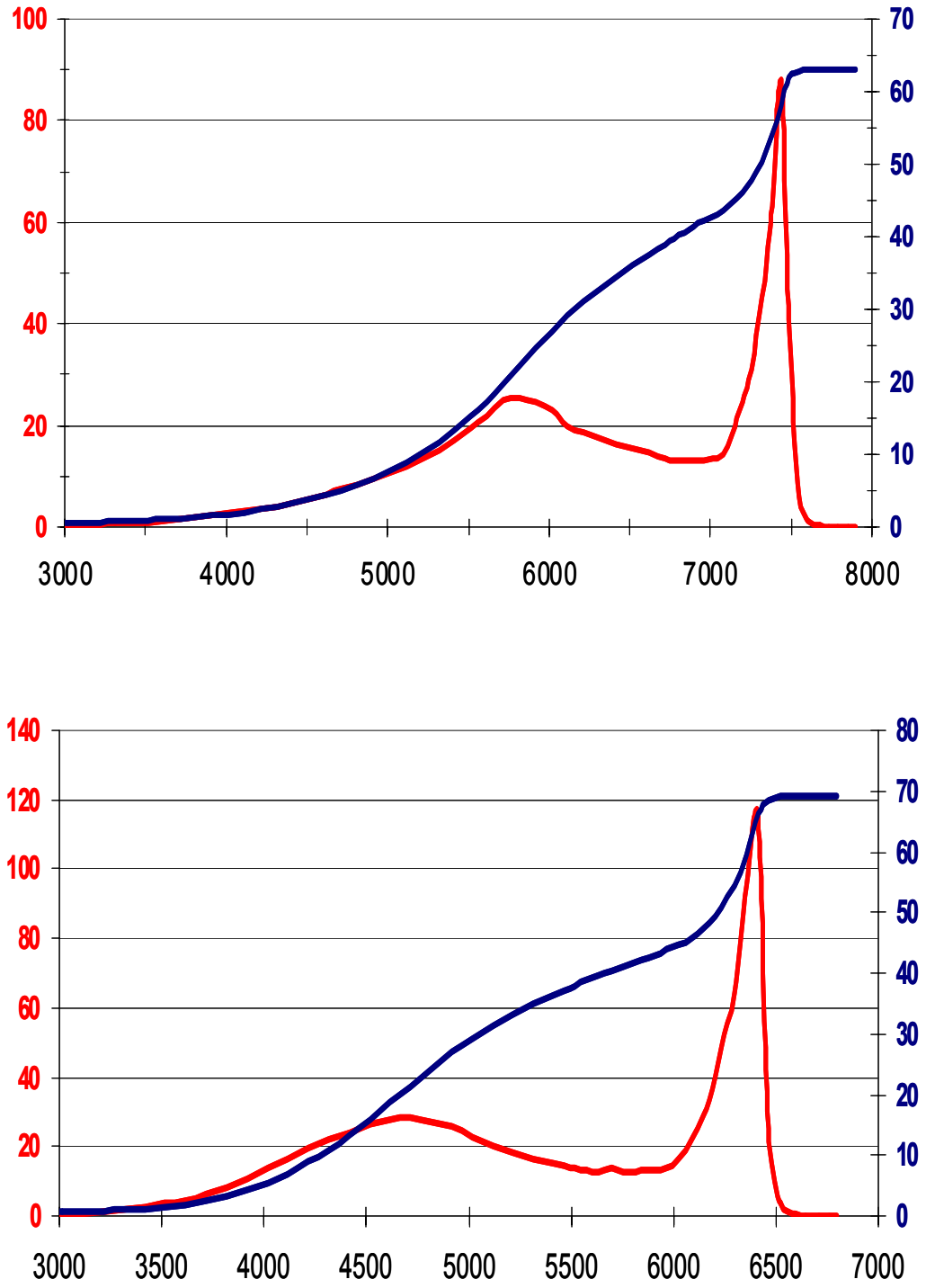

Fig. 42: UPM: total hydrogen production for cases 1 and 2

The figure shows results for case 1 (top) and case 2 (bottom). Red curves refer to the rate in mg/s and blue ones to the total accumulated mass in g.

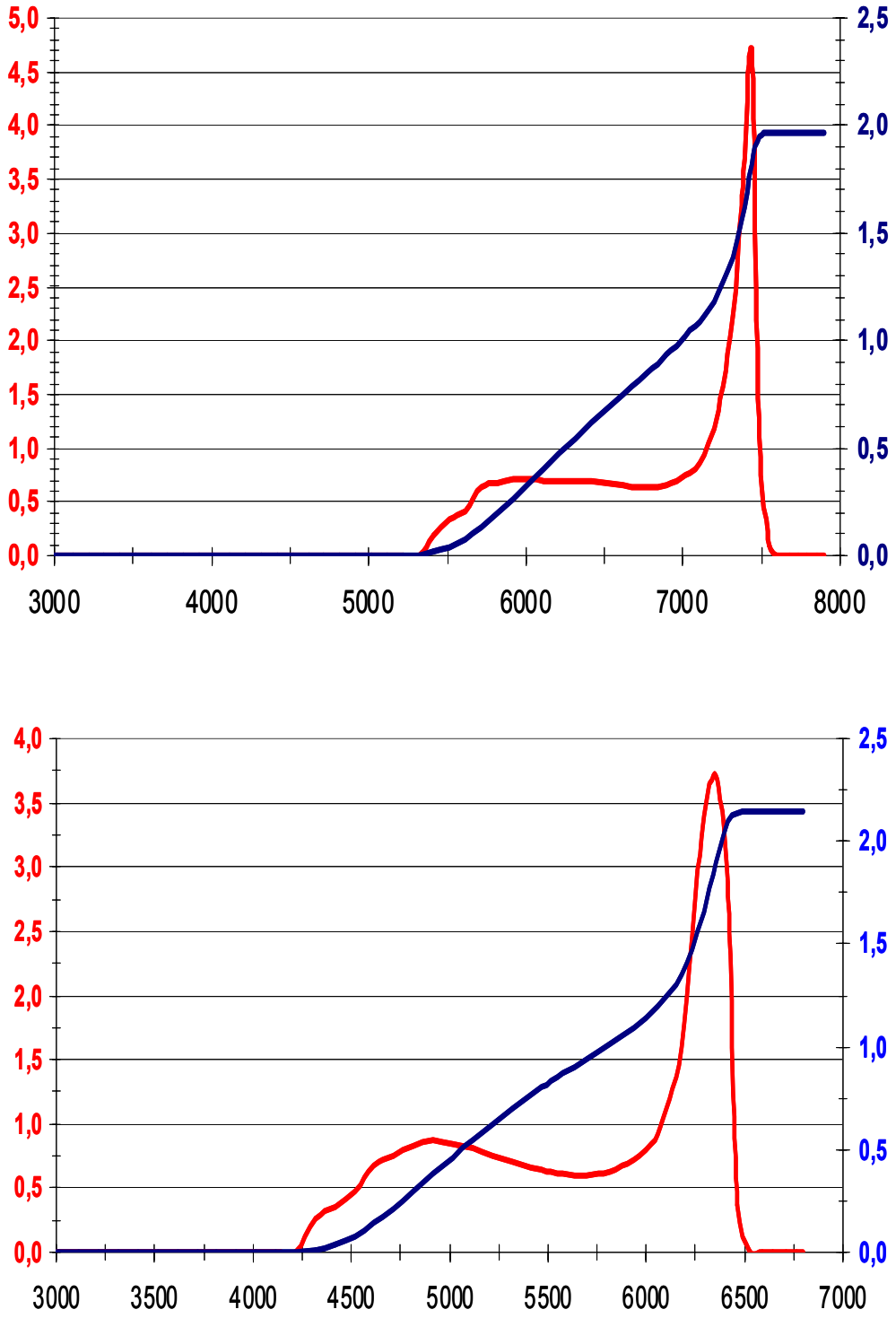

Fig. 43: UPM: H_2 generation due to B_4C oxidation for cases 1 and 2

The figure shows results for case 1 (top) and case 2 (bottom). Red curves refer to the rate in mg/s and blue ones to the total accumulated mass in g.

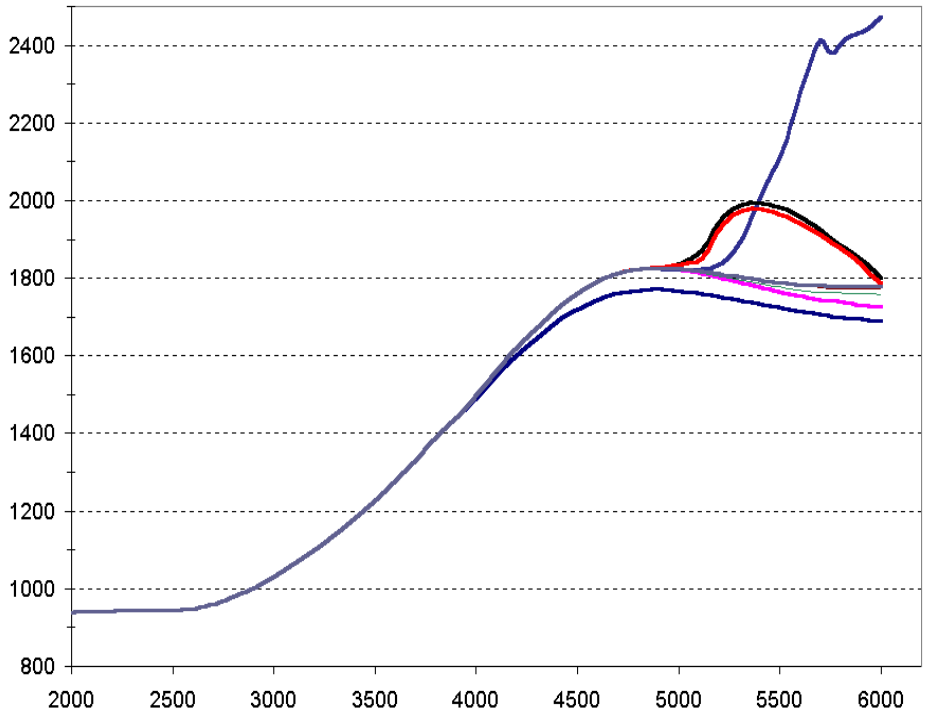

Fig. 44: UPM: sensitivity of the thermal response to the electric power (cases 1 and 2)